Transactions on Fuzzy Sets and Systems

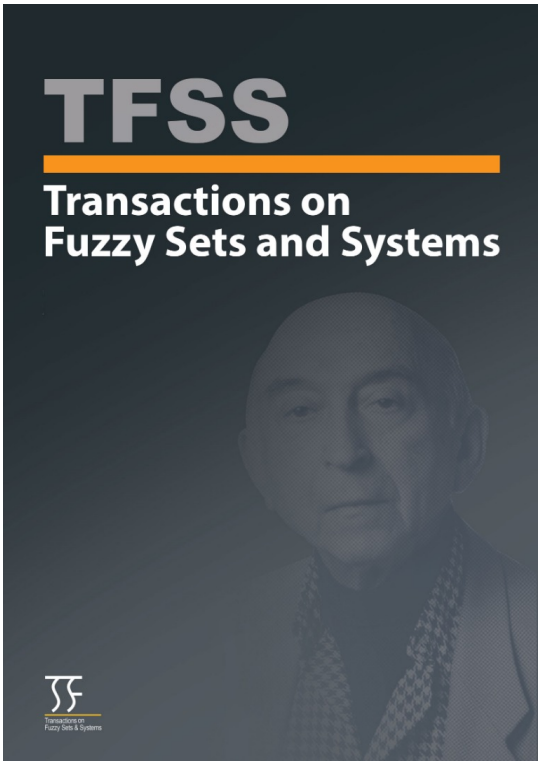

Transactions on Fuzzy Sets and Systems

ISSN: **2821-0131**

https://sanad.iau.ir/journal/tfss/

Enhanced Modelling of Listeriosis Disease Transmission Using Fractal-Fractional Differential Equations with Fuzzy Logic

Vol.5, No.2, (2026), 85-111. DOI: https://doi.org/10.71602/tfss.2026.1193187

Author(s):

Tamil Vizhi Mariappan, Department of Mathematics, Alagappa University, Karaikudi, India.
E-mail: tamilvizhi2502@gmail.com
Vimala Jayakumar, Department of Mathematics, Alagappa University, Karaikudi, India.
E-mail: vimaljey@alagappauniversity.ac.in
Jeevitha Kannan, Department of Mathematics, Alagappa University, Karaikudi, India.
E-mail: kjeevitha991@gmail.com

Transactions on Fuzzy Sets and Systems (TFSS)
URL: https://sanad.iau.ir/journal/tfss/
Online ISSN: 2821-0131
Vol.5, No.2, (2026), 85-111
DOI: https://doi.org/10.71602/tfss.2026.1193187

Article Type: Original Research Article
(Journal Pre-proof)

Enhanced Modelling of Listeriosis Disease Transmission Using Fractal-Fractional Differential Equations with Fuzzy Logic

Tamil Vizhi Mariappan, **Vimala Jayakumar***, **Jeevitha Kannan**

Abstract. Listeriosis, caused by *Listeria monocytogenes*, presents significant public health risks, especially to vulnerable groups such as the elderly, immunocompromised individuals, and pregnant women. Despite advancements in food safety measures, the bacteria's resilience across various environments makes their complete eradication challenging. This study addresses this challenge by incorporating uncertainty and memory effects into the disease modelling process. This study offers an advanced mathematical framework to analyse listeriosis dynamics using fractal-fractional differential equations and a fuzzy fractal-fractional approach. The integration of fractal calculus allows for a detailed examination of complex, multi-scale behaviours of real-world disease spread, while the incorporation of fuzzy logic accounts for inherent uncertainties in initial conditions and parameter values. Ensuring the mathematical validity of the proposed models, the research explores key properties such as existence, uniqueness, and Ulam-Hyers stability, which confirm the robustness and reliability of the solutions. A computational approach is utilized to solve the model, revealing the dynamics of susceptible, infected, and recovered populations, as well as the bacterial class and the progression of spoiled and unspoiled food packages over time. The importance of fractal dimensions in the Listeriosis model is emphasized by variation maps that depict changes over time. The extension of the model to include fuzzy initial conditions enhances predictive capabilities and supports decision-making by accommodating uncertainty. The findings underscore the importance of applying sophisticated mathematical tools, such as fractal-fractional and fuzzy differential equations, to improve the understanding and management of listeriosis and similar public health challenges, enabling more effective prevention and control strategies.

AMS Subject Classification 2020: 34A07; 34K36
Keywords and Phrases: Listeriosis disease, Ulam-Hyers stable, Riemann-Liouville fractal-fractional derivative, Lagrange piecewise interpolation, fuzzy number.

1 Introduction

The bacterium *Listeria monocytogenes*, which primarily transmits through contaminated foods like soft cheeses, deli meats, and other ready-to-eat products, causes listeriosis, a life-threatening disease [1, 2]. This pathogen poses a particularly high risk to vulnerable groups, including the elderly, immunocompromised individuals, and pregnant women, often resulting in severe manifestations like sepsis and meningitis, with a case-fatality rate ranging from 20-30% even with treatment [3, 4, 5, 6].

Recent advances in food safety practices, such as Hazard Analysis and Critical Control Points (HACCP) principles, along with improved microbiological testing, have reduced the incidence of sporadic listeriosis

∗**Corresponding Author:** Vimala Jayakumar, Email: vimaljey@alagappauniversity.ac.in, ORCID: 0000-0003-3138-9365
Received: 11 December 2024; **Revised**: 3 July 2025; **Accepted**: 5 July 2025; **Available Online**: 1 August 2025; **Published Online**: 7 November 2026.

How to cite: Tamil Vizhi Mariappan, Vimala Jayakumar, Jeevitha Kannan. Enhanced modelling of Listeriosis Disease Transmission Using Fractal-Fractional Differential Equations with Fuzzy Logic. *Transactions on Fuzzy Sets and Systems.* 2026; 5(2): 85-111. DOI: https://doi.org/10.71602/tfss.2026.1193187

in industrialized nations [7, 8, 9, 10]. However, complete eradication remains challenging due to its ability to thrive in diverse environmental conditions, displaying resilience in cold temperatures and high-salt environments, which facilitates its survival and persistence within the food supply chain [11, 12, 13]. The intricate epidemiology of *L. monocytogenes*, combined with its pervasive presence and adaptability, highlights the necessity for advanced modelling techniques to forecast the pathogen's behaviour, enhance prevention strategies, and control its transmission dynamics in human populations [14, 15].

Mathematical modelling is crucial for understanding and controlling listeriosis, and recent researchers [16, 17, 18] have extensively explored the study of foodborne pathogens and antimicrobial resistance at the farm level. A mechanistic dose-response model incorporating biological factors like gastric acid and immune response improved experimental design in understanding infection dynamics [19, 20]. Another study [21, 22] addressed cross-contamination in food processing environments, emphasizing the need for stringent hygiene practices. A multi-population model [23] included vulnerable groups, such as pregnant women and newborns, and examined food and environmental contamination routes. An innovative framework [24] for identifying contaminated products during foodborne outbreaks used retail sales data, facilitating early intervention and limiting listeriosis spread. The use of fractional calculus in modelling infection dynamics, particularly for listeriosis, provided a more nuanced understanding of pathogen persistence compared to traditional models [25, 26]. These research efforts highlight the value of advanced mathematical models, especially fractional calculus, in improving the understanding and management of foodborne infections and antimicrobial resistance.

Fractal-fractional differential equations are a powerful tool in mathematical modelling, combining fractional calculus and fractal geometry. They provide a more accurate representation of complex phenomena in fields like physics, engineering, biology, and economics. The foundation of fractal-fractional calculus [27] lies in the extension of traditional calculus to non-integer orders and the incorporation of fractal dimensions. This approach allows for the description of memory effects, non-local interactions, and self-similarity in natural and artificial systems. Key advantages of using fractal-fractional differential equations include enhanced accuracy, flexibility, and multiscale modelling.

The development of fractal-fractional differential equations has significantly enhanced mathematical modelling, particularly evident in analyses like the monkeypox outbreak in the United States from May 2022 to May 2023 [28]. Numerical results highlighted the importance of fractal-fractional order in accurately fitting real data [29]. In related research [30], a fractal-fractional model was validated against viral diarrhoea data from 2008 to 2018, utilizing a fractional order of 0.85 and a fractal order of 0.62. Recent studies [31, 32] have increasingly employed fractal-fractional operators, showcasing their superior accuracy compared to traditional models, particularly with SARS-CoV-2 data in Pakistan and diabetes patient data. Additionally, a new fractal-fractional MSEIR model [33, 34] was introduced to analyse the chickenpox outbreak among Shenzhen school children in 2013, indicating that the fractal-fractional model offers a more precise representation of disease dynamics than classical and other fractional-order models.

Incorporating fuzzy logic within the mathematical framework allows for the representation of uncertainties, enhancing the model's ability to produce realistic simulations and inform decision-making processes. Addressing the inherent uncertainty in initial conditions and parameter variability is crucial, as real-world data often exhibit imprecision that traditional models cannot accommodate effectively. The author [35] investigates fuzzy fractional operators and provides a comprehensive evaluation of these operators and the corresponding fuzzy fractional equations, emphasizing the importance of incorporating fuzzy logic in modelling. The authors [36, 37] developed fuzzy fractional differential equations for fuzzy HIV and COVID-19 modelling. They have established the uniqueness of their solution and provided numerical simulations to demonstrate its effectiveness. Some authors [38, 39] presented a numerical method for solving a fuzzy AH1N1/09 influenza model and developed a fuzzy fractional Caputo derivative approach for modelling the SIR dynamics of childhood diseases.

1.1 Motivation

- Listeriosis poses significant public health risks, particularly among vulnerable groups, and presents difficulties for food safety and public health monitoring due to its thriving environment.
- Current epidemiological models often fall short in capturing the intricate transmission pathways and environmental persistence of *L. monocytogenes*, leading to gaps in predictive capabilities and control strategies.
- Mathematical modelling using conventional differential equations may not fully represent the non-linear, fractal-like patterns observed in real-world listeriosis outbreaks.
- Fractal-fractional differential equations provide a means to model complex, multi-scale behaviours inherent to the transmission and spread of listeriosis, offering a more accurate depiction of the disease dynamics.
- Fuzzy logic in the Listeria models further enhances simulations and decision-making by representing uncertainties in the initial conditions and addressing imprecision in real-world data.
- Improved predictive models are vital for designing targeted intervention strategies and resource allocation to prevent and mitigate listeriosis outbreaks, thereby reducing public health risks.
- The combination of advanced mathematical approaches, such as fractal-fractional calculus and fuzzy modelling, aligns with the need for sophisticated tools that can handle complex biological and epidemiological systems.

1.2 Objectives

- Develop a comprehensive mathematical model using fractal-fractional differential equations to analyse the complex dynamics of listeriosis.
- Integrate fuzzy logic to incorporate uncertainties in initial conditions and parameter variability for more robust predictions.
- Study key mathematical properties, including existence, uniqueness, and Ulam-Hyers stability, to ensure the reliability and soundness of the model.
- Examine the impact of fractional orders and fractal dimensions on the dynamics of listeriosis to identify critical factors influencing disease spread.
- Provide a refined tool for public health officials and researchers to design better intervention and control strategies.

1.3 Manuscript Framework

Section 2 provides the fundamental definitions that set the groundwork for the study. This manuscript is organized into two main parts:

Part 1: Fractal-Fractional Model

- **Section 3**: Presents the formulation of the Listeriosis disease model and introduces the fractal-fractional Listeriosis model, accompanied by an in-depth analysis.

- **Section 4**: Addresses the existence and uniqueness of the model's solutions, ensuring mathematical rigor.
- **Section 5**: Discusses the Ulam-Hyers stability, which evaluates the model's resilience under small perturbations.
- **Section 6**: Outlines the computational scheme utilizing Lagrange piecewise interpolation.
- **Subsection 6.1**: Examines the model's results and solutions through simulations and graphical representations.
- **Subsection 6.2**: Explains why fractal dimensions are important for the model and includes variation maps to show their effects clearly.

Part 2: Fuzzy Fractal-Fractional Model

- **Section 7**: Introduces the fractal-fractional Listeriosis model and uses the computational framework from Section 6 to find its solutions.
- **Subsection 7.1**: Discusses the simulations and results obtained from this model, supported by illustrative figures.

2 Basic Concepts

Definition 2.1. [27] *A function* $m(\mathrm{t})$ *is fractal differentiable with fractal order* ϑ *on (a,b) if* $\frac{dm(\mathrm{t})}{dt^{\vartheta}} = \lim_{\mathrm{v}\to\mathrm{t}} \frac{m(\mathrm{v})-m(t)}{\mathrm{v}^{\vartheta}-t^{\vartheta}}$ *exists.*

Definition 2.2. [29] *The fractal-fractional derivative of a fractal differentiable* $m(\mathrm{t})$ *function on (a,b), in Riemann-Liouville sense with fractional order* ς *is represented as:*

$$^{\varsigma,\vartheta}\mathfrak{D}(m(\mathrm{t})) = \frac{\Delta(\varsigma)}{1-\varsigma}\frac{d}{d\mathrm{t}^{\vartheta}}\int_0^{\mathrm{t}} \mathrm{E}_{\varsigma}\left[-\frac{\varsigma}{1-\varsigma}(\mathrm{t}-\mathrm{v})^{\varsigma}\right]m(\mathrm{v})d\mathrm{v}, \tag{1}$$

Here, $\Delta(\varsigma) = 1 - \varsigma + \frac{\varsigma}{\Gamma(\varsigma)}$ is the normalizer function and Mittag-Leffler Kernel is $\mathrm{E}_{\varsigma}(\mathrm{t}) = \sum_{n=0}^{\infty} \frac{\mathrm{t}^n}{\alpha \mathrm{t}+1}$.

Definition 2.3. [34] *The Atangana-Baleanu fractional derivative of* $m(\mathrm{t})$ *function on (a,b) with fractional order* ς *in Riemann-Liouville sense is represented as:*

$$^{\varsigma}\mathfrak{D}(m(\mathrm{t})) = \frac{\Delta(\varsigma)}{1-\varsigma}\frac{d}{dt}\int_0^{\mathrm{t}} \mathrm{E}_{\varsigma}\left[-\frac{\varsigma}{1-\varsigma}(\mathrm{t}-\mathrm{v})^{\varsigma}\right]m(\mathrm{v})d\mathrm{v} \tag{2}$$

The fractional integral of $m(\mathrm{t})$ *is represented as:*

$$^{\varsigma}\mathfrak{I}(m(\mathrm{t})) = \frac{1-\varsigma}{\Delta(\varsigma)}m(\mathrm{t}) + \frac{\varsigma}{\Delta(\varsigma)\Gamma(\varsigma)}\int_0^{\mathrm{t}}(\mathrm{t}-\mathrm{v})^{\varsigma-1}m(\mathrm{v})d\mathrm{v} \tag{3}$$

Definition 2.4. [36] *The parametric form of a fuzzy number* $\tilde{m}$ *is represented by* $[\tilde{m}]_{\alpha} = [\tilde{m}^{-}(\alpha),\tilde{\mathrm{m}}^{+}(\alpha)]$, *where* $0 \le \alpha \le 1$ *and the functions* $\tilde{m}^{-}(\alpha)$ *and* $\tilde{m}^{+}(\alpha)$ *satisfies the below conditions:*

- $\tilde{m}^{-}(\alpha)$ *is non-decreasing bounded right continuous at zero and left continuous function for other values of* α.

- $\tilde{m}^{-}(\alpha)$ *is non-increasing bounded right continuous at zero and a left-continuous function for other values of* α.
- *For all* α, $\tilde{m}^{+}(\alpha) \geq \tilde{m}^{-}(\alpha)$.

Definition 2.5. [35, 36] *For fuzzy numbers* $\tilde{m}_1$, $\tilde{m}_2$ *and* $\tilde{m}_3$, *the arithmetic operations are defined by*

- $[\tilde{m}_1 \oplus \tilde{m}_2]_\alpha = [\tilde{m}_1^{-}(\alpha) + \tilde{m}_2^{-}(\alpha),\ \tilde{m}_1^{+}(\alpha) + \tilde{m}_2^{+}(\alpha)]$,
- *For* $\mathrm{g} \in \Re$, $[\mathrm{g} \odot \tilde{m}]_\alpha = \begin{cases} [g\tilde{m}^{-}(\alpha), g\tilde{m}^{+}(\alpha)], & \text{if } \mathrm{g} \geq 0 \\ [g\tilde{m}^{+}(\alpha), g\tilde{m}^{-}(\alpha)], & \text{if } g < 0, \end{cases}$
- $\tilde{m}_1 \ominus \tilde{m}_2 = \tilde{m}_3 \iff \begin{cases} (i)\tilde{m}_1 = \tilde{m}_2 \oplus \tilde{m}_3, \\ (ii)\tilde{m}_2 = \tilde{m}_1 \oplus (-1)\tilde{m}_3. \end{cases}$

  i.e. $[\tilde{m}_1]_\alpha \ominus [\tilde{m}_2]_\alpha = [\min\{\tilde{m}_1^{-}(\alpha) - \tilde{m}_2^{-}(\alpha), \tilde{m}_1^{+}(\alpha) - \tilde{m}_2^{+}(\alpha)\}, \max\{\tilde{m}_1^{-}(\alpha) - \tilde{m}_2^{-}(\alpha), \tilde{m}_1^{+}(\alpha) - \tilde{m}_2^{+}(\alpha)\}]$

where $\ominus$ *is the GH-difference (generalized Hukuhara difference).*

Definition 2.6. [36] *A fuzzy-valued function* $\tilde{m}(\mathrm{t})$ *is GH-differentiable at* $\mathrm{t} \in (a,b)$ *if* $\frac{d\tilde{m}(\mathrm{t})}{d\mathrm{t}} = \lim_{\mathrm{h}\to 0} \frac{1}{\mathrm{h}}[\tilde{m}(\mathrm{t}+\mathrm{h}) \ominus \tilde{m}(\mathrm{t})]$ *exists.*

3 Fractal-Fractional Listeriosis Model

The mathematical framework for Listeriosis disease models captures the interactions among three key groups: the human population, food products (both unspoiled and spoiled), and environmental *L. Monocytogenes* bacteria.

1. Dynamics of Human Population:
   - The human population consists of three variables: Susceptible $\mathcal{H}_s$, Infected $\mathcal{H}_i$, and Recovered $\mathcal{H}_r$, following the *SIR* framework.
   - The total population at any time $\mathcal{H}(\mathrm{t}) = \mathcal{H}_s(\mathrm{t}) + \mathcal{H}_i(\mathrm{t}) + \mathcal{H}_r(\mathrm{t})$.
   - Infection Pathways: (1) Food Ingestion - Listeria transmission occurs when humans ingest spoiled food, influenced by contact rate ρ_1. (2) Environmental Exposure - Individuals can also be infected through direct environmental exposure to Listeria bacteria, governed by contact rate ρ_2.
   - Infection Rate ${}^{*}\lambda$: The rate of new infections is calculated with food ingestion and environmental exposure.
   - After infection, individuals recover at rate δ_2, but they can return to susceptibility over time at a rate δ_1.
   - The human population mortality rate τ, which accounts for deaths and transmission rate from susceptible to infected, is λ.
2. Environmental Bacteria:
   - Logistic Growth: The Listeria population $\mathcal{L}$ in the environment follows a logistic growth $\frac{d\mathcal{L}}{dt} = \sigma\mathcal{L}\left(1 - \frac{\mathcal{L}}{\delta_3}\right)$, where σ is the growth rate and δ_3 is the load capacity of the environment.
   - Environmental Factors: The environment influences infection rates by determining the level of Listeria present, which then affects food contamination.

Table 1: Description of parameters and their values

Parameters	**Representation**	**Values**
τ	Rate of natural mortalities	$1/(65\times360)$
μ	Production rate of unspoiled food	0.0076
δ_2	Rate of recovery	0.0094
σ	Aggregate growth rate of $\mathcal{L}$	0.02
ρ_1	Rate of Listeriosis human infection via unspoiled food	0.038
ρ_2	Food spoiled rate by Listeriosis bacteria	0.002
ρ_3	Spoiled rate of unspoiled food products	0.0005
δ_1	Rate of immunity depletion	0.09

3. Food Spoliation Dynamics:

- Food is classified into unspoiled $\mathcal{U}$ and spoiled $\mathcal{C}$ categories, with the total food supply $\mathcal{F} = \mathcal{U} + \mathcal{C}$.

- Food Spoliation Rate ${}^*\eta$ is calculated from ρ_2 and ρ_3, where they are contact rates affecting contamination in the environment and food processing facilities, respectively.

- Food Production: Uncontaminated food is produced at a rate μ, and contamination occurs at a rate η through environmental exposure and food handling.

The comprehensive flowchart illustrating the Listeriosis disease model, as depicted in Figure 1, provides a detailed schematic representation of the interactions and processes involved in the progression of the disease. Additionally, Table 1 offers an exhaustive description of the model's parameters, encompassing their respective definitions and assumed quantitative values.

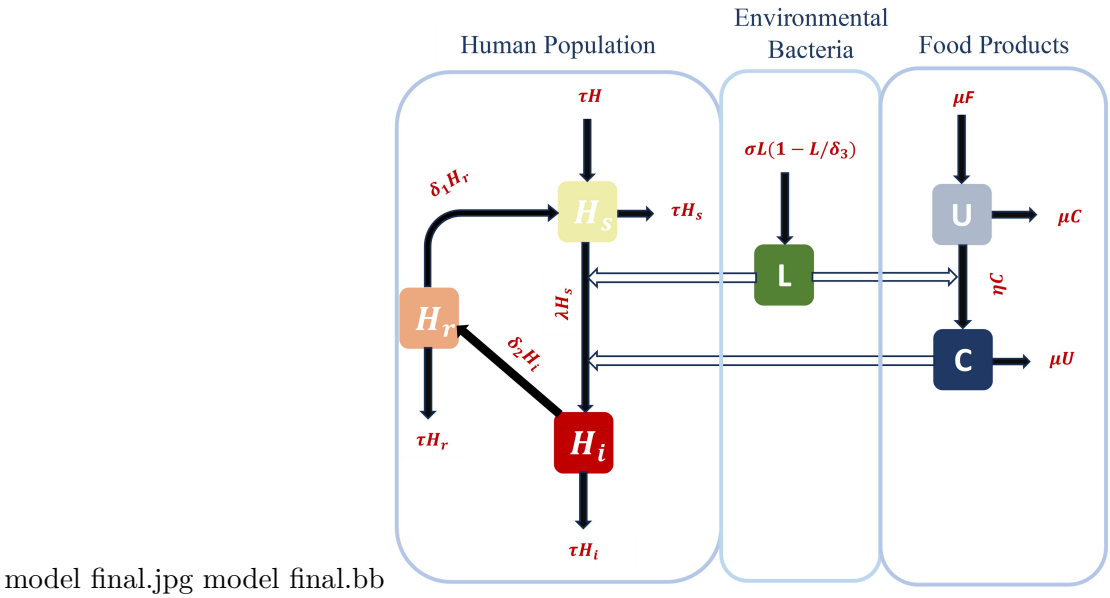

model final.jpg model final.bb

Figure 1: Flow-Chart of Listeriosis Disease Model - Dark black arrows represent the transmission within each group, and empty arrows represent the transmission among other groups.

The following formulation presents the ordinary differential equation model for Listeriosis, as initially introduced by [16]. This model encapsulates the dynamic interactions between various biological categories and pathways pertinent to the transmission and progression of Listeriosis. The equations are designed to mathematically represent the changes over time within the system, thereby facilitating in-depth analysis of the epidemiological behaviour and potential intervention strategies.

$$
\begin{aligned}
\frac{d\mathcal{H}_s}{dt} &= \tau\mathcal{H} + \delta_3\mathcal{H}_r - (\lambda+\tau)\mathcal{H}_s \\
\frac{d\mathcal{H}_i}{dt} &= \lambda\mathcal{H}_s - (\delta_2+\tau)\mathcal{H}_i \\
\frac{d\mathcal{H}_r}{dt} &= \delta_2\mathcal{H}_i - (\delta_1+\tau)\mathcal{H}_r \\
\frac{d\mathcal{L}}{dt} &= \sigma\mathcal{L}\Big(1-\frac{\mathcal{L}}{\delta_3}\Big) \\
\frac{d\mathcal{U}}{dt} &= \mu\mathcal{F} - (\eta+\mu)\mathcal{U} \\
\frac{d\mathcal{C}}{dt} &= \eta\mathcal{U} - \mu\mathcal{C}
\end{aligned}
\tag{4}
$$

Eliminating $\mathcal{H}_r(t) = \mathcal{H}(\mathrm{t})$ - $\mathcal{H}_s(\mathrm{t})$ - $\mathcal{H}_i(\mathrm{t})$ and taking $\mathfrak{s} = \frac{\mathcal{H}_s}{\mathcal{H}}$, $\mathfrak{i} = \frac{\mathcal{H}_i}{\mathcal{H}}$, $\mathfrak{l} = \frac{\mathcal{L}}{\delta_3}$, $\mathfrak{u} = \frac{\mathcal{U}}{\mathcal{F}}$, $\mathfrak{c} = \frac{\mathcal{C}}{\mathcal{F}}$.
Thus (4) simplified as

$$\begin{aligned}
\frac{d\mathfrak{s}}{d\mathrm{t}} &= \tau + \delta_1(1-\mathfrak{s}-\mathfrak{i}) - ({}^*\lambda + \tau)\mathfrak{s} \\
\frac{d\mathfrak{i}}{d\mathrm{t}} &= ({}^*\lambda)\mathfrak{s} - (\delta_2 + \tau)\mathfrak{i} \\
\frac{d\mathfrak{l}}{d\mathrm{t}} &= \sigma\mathfrak{l}(1-\mathfrak{l}) \\
\frac{d\mathfrak{u}}{d\mathrm{t}} &= \mu - ({}^*\eta + \mu)\mathfrak{u} \\
\frac{d\mathfrak{c}}{d\mathrm{t}} &= ({}^*\eta)\mathfrak{u} - \mu\mathfrak{c}
\end{aligned} \tag{5}$$

where ${}^*\lambda = \rho_1\mathfrak{c} + \rho_2\mathfrak{l}$ and ${}^*\eta = \rho_2\mathfrak{l} + \rho_3\mathfrak{c}$.
Fractal-fractional order Listeriosis disease model can be written as:

$$\begin{aligned}
{}^{\varsigma,\vartheta}\mathfrak{D}(\mathfrak{s}) &= \tau^{\vartheta+\varsigma-1} + \delta_1^{\vartheta+\varsigma-1}(1-\mathfrak{s}-\mathfrak{i}) - ({}^*\lambda^{\vartheta+\varsigma-1} + \tau^{\vartheta+\varsigma-1})\mathfrak{s} \\
{}^{\varsigma,\vartheta}\mathfrak{D}(\mathfrak{i}) &= ({}^*\lambda)^{\vartheta+\varsigma-1}\mathfrak{s} - (\delta_2^{\vartheta+\varsigma-1} + \tau^{\vartheta+\varsigma-1})\mathfrak{i} \\
{}^{\varsigma,\vartheta}\mathfrak{D}(\mathfrak{l}) &= \sigma^{\vartheta+\varsigma-1}\mathfrak{l}(1-\mathfrak{l}) \\
{}^{\varsigma,\vartheta}\mathfrak{D}(\mathfrak{u}) &= \mu^{\vartheta+\varsigma-1} - ({}^*\eta^{\vartheta+\varsigma-1} + \mu^{\vartheta+\varsigma-1})\mathfrak{u} \\
{}^{\varsigma,\vartheta}\mathfrak{D}(\mathfrak{c}) &= ({}^*\eta)^{\vartheta+\varsigma-1}\mathfrak{u} - \mu^{\vartheta+\varsigma-1}\mathfrak{c}
\end{aligned} \tag{6}$$

To address the dimensional mismatch in the fractal derivative, the condition $\vartheta + \varsigma - 1 = \epsilon$ is applied. Then the model (6) can be formulated as:

$$\begin{aligned}
{}^{\varsigma,\vartheta}\mathfrak{D}(\mathfrak{s}) &= \tau^{\epsilon} + \delta_1^{\epsilon}(1-\mathfrak{s}-\mathfrak{i}) - ({}^*\lambda^{\epsilon} + \tau^{\epsilon})\mathfrak{s} \\
{}^{\varsigma,\vartheta}\mathfrak{D}(\mathfrak{i}) &= ({}^*\lambda)^{\epsilon}\mathfrak{s} - (\delta_2^{\epsilon} + \tau^{\epsilon})\mathfrak{i} \\
{}^{\varsigma,\vartheta}\mathfrak{D}(\mathfrak{l}) &= \sigma^{\epsilon}\mathfrak{l}(1-\mathfrak{l}) \\
{}^{\varsigma,\vartheta}\mathfrak{D}(\mathfrak{u}) &= \mu^{\epsilon} - ({}^*\eta^{\epsilon} + \mu^{\epsilon})\mathfrak{u} \\
{}^{\varsigma,\vartheta}\mathfrak{D}(\mathfrak{c}) &= ({}^*\eta)^{\epsilon}\mathfrak{u} - \mu^{\epsilon}\mathfrak{c}
\end{aligned} \tag{7}$$

along with the initial conditions $\mathfrak{s}(0) = \mathfrak{s}_0$, $\mathfrak{i}(0) = \mathfrak{i}_0$, $\mathfrak{l}(0) = \mathfrak{l}_0$, $\mathfrak{u}(0) = \mathfrak{u}_0$ and $\mathfrak{c}(0) = \mathfrak{c}_0$; where $0 \leq \mathfrak{s}_0, \mathfrak{i}_0, \mathfrak{l}_0, \mathfrak{u}_0, \mathfrak{c}_0 \leq 1$; $0 < \varsigma, \vartheta \leq 1$ and $\mathrm{t} \in I = [0, T]$.

4 Existence and Uniqueness

It is essential to rigorously verify the existence and uniqueness of solutions for the proposed models to ensure their mathematical validity and reliability. In this context, we establish the existence of solutions by applying Schauder's Fixed Point Theorem [40], which provides a foundational basis for demonstrating that solutions exist under certain continuity and compactness conditions. Furthermore, the uniqueness of the solutions is proven through Banach's Fixed Point Theorem [40], which ensures that, given specific contractive properties, the solution is singular and stable. This dual approach of confirming both existence and uniqueness strengthens the theoretical framework of the model and supports its application to real-world scenarios.
Define a Banach space $\Omega = \{(\mathfrak{s}, \mathfrak{i}, \mathfrak{l}, \mathfrak{u}, \mathfrak{c}) \in \mathbb{R}_+^5 \mid 0 \leq \mathfrak{s} + \mathfrak{i} \leq 1;\ 0 \leq \mathfrak{l} \leq 1; 0 \leq \mathfrak{u} + \mathfrak{c} \leq 1\}$ with norm $\| \psi \| = \max_{\mathrm{t} \in I} \left(|\mathfrak{s}(\mathrm{t})| + |\mathfrak{i}(\mathrm{t})| + |\mathfrak{l}(\mathrm{t})| + |\mathfrak{u}(\mathrm{t})| + |\mathfrak{c}(\mathrm{t})|\right)$.

From the model (7), we can represent the functions as

$$\begin{aligned}
\psi_1(t,\mathfrak{s},\mathfrak{i},\mathfrak{l},\mathfrak{u},\mathfrak{c}) &= \tau^{\epsilon} + \delta_1^{\epsilon}(1-\mathfrak{s}-\mathfrak{i}) - ({}^{*}\lambda^{\epsilon}+\tau^{\epsilon})\mathfrak{s}\\
\psi_2(t,\mathfrak{s},\mathfrak{i},\mathfrak{l},\mathfrak{u},\mathfrak{c}) &= ({}^{*}\lambda)^{\epsilon}\mathfrak{s} - (\delta_2^{\epsilon}+\tau^{\epsilon})\mathfrak{i}\\
\psi_3(t,\mathfrak{s},\mathfrak{i},\mathfrak{l},\mathfrak{u},\mathfrak{c}) &= \sigma^{\epsilon}\mathfrak{l}(1-\mathfrak{l})\\
\psi_4(t,\mathfrak{s},\mathfrak{i},\mathfrak{l},\mathfrak{u},\mathfrak{c}) &= \mu^{\epsilon} - ({}^{*}\eta^{\epsilon}+\mu^{\epsilon})\mathfrak{u}\\
\psi_5(t,\mathfrak{s},\mathfrak{i},\mathfrak{l},\mathfrak{u},\mathfrak{c}) &= ({}^{*}\eta)^{\epsilon}\mathfrak{u} - \mu^{\epsilon}\mathfrak{c}
\end{aligned} \tag{8}$$

Considering the relation between fractal derivative and ordinary derivative, we can express (7) as:

$$\begin{aligned}
{}^{\varsigma}\mathfrak{D}(\mathfrak{s}(t)) &= \vartheta t^{\vartheta-1}\psi_1(t,\mathfrak{s},\mathfrak{i},\mathfrak{l},\mathfrak{u},\mathfrak{c})\\
{}^{\varsigma}\mathfrak{D}(\mathfrak{i}(t)) &= \vartheta t^{\vartheta-1}\psi_2(t,\mathfrak{s},\mathfrak{i},\mathfrak{l},\mathfrak{u},\mathfrak{c})\\
{}^{\varsigma}\mathfrak{D}(\mathfrak{l}(t)) &= \vartheta t^{\vartheta-1}\psi_3(t,\mathfrak{s},\mathfrak{i},\mathfrak{l},\mathfrak{u},\mathfrak{c})\\
{}^{\varsigma}\mathfrak{D}(\mathfrak{u}(t)) &= \vartheta t^{\vartheta-1}\psi_4(t,\mathfrak{s},\mathfrak{i},\mathfrak{l},\mathfrak{u},\mathfrak{c})\\
{}^{\varsigma}\mathfrak{D}(\mathfrak{c}(t)) &= \vartheta t^{\vartheta-1}\psi_5(t,\mathfrak{s},\mathfrak{i},\mathfrak{l},\mathfrak{u},\mathfrak{c})
\end{aligned} \tag{9}$$

Taking fractional integration (3) on both sides, we obtain

$$\begin{aligned}
\mathfrak{s}(t) &= \mathfrak{s}_0 + \frac{(1-\varsigma)\vartheta t^{\vartheta-1}}{\Delta(\varsigma)}\psi_1(t,\mathfrak{s},\mathfrak{i},\mathfrak{l},\mathfrak{u},\mathfrak{c}) + \frac{\varsigma\vartheta}{\Delta(\varsigma)\Gamma(\varsigma)}\int_0^t v^{\vartheta-1}(t-v)^{\varsigma-1}\psi_1(v,\mathfrak{s},\mathfrak{i},\mathfrak{l},\mathfrak{u},\mathfrak{c})dv\\
\mathfrak{i}(t) &= \mathfrak{i}_0 + \frac{(1-\varsigma)\vartheta t^{\vartheta-1}}{\Delta(\varsigma)}\psi_2(t,\mathfrak{s},\mathfrak{i},\mathfrak{l},\mathfrak{u},\mathfrak{c}) + \frac{\varsigma\vartheta}{\Delta(\varsigma)\Gamma(\varsigma)}\int_0^t v^{\vartheta-1}(t-v)^{\varsigma-1}\psi_2(v,\mathfrak{s},\mathfrak{i},\mathfrak{l},\mathfrak{u},\mathfrak{c})dv\\
\mathfrak{l}(t) &= \mathfrak{l}_0 + \frac{(1-\varsigma)\vartheta t^{\vartheta-1}}{\Delta(\varsigma)}\psi_3(t,\mathfrak{s},\mathfrak{i},\mathfrak{l},\mathfrak{u},\mathfrak{c}) + \frac{\varsigma\vartheta}{\Delta(\varsigma)\Gamma(\varsigma)}\int_0^t v^{\vartheta-1}(t-v)^{\varsigma-1}\psi_3(v,\mathfrak{s},\mathfrak{i},\mathfrak{l},\mathfrak{u},\mathfrak{c})dv\\
\mathfrak{u}(t) &= \mathfrak{u}_0 + \frac{(1-\varsigma)\vartheta t^{\vartheta-1}}{\Delta(\varsigma)}\psi_4(t,\mathfrak{s},\mathfrak{i},\mathfrak{l},\mathfrak{u},\mathfrak{c}) + \frac{\varsigma\vartheta}{\Delta(\varsigma)\Gamma(\varsigma)}\int_0^t v^{\vartheta-1}(t-v)^{\varsigma-1}\psi_4(v,\mathfrak{s},\mathfrak{i},\mathfrak{l},\mathfrak{u},\mathfrak{c})dv\\
\mathfrak{c}(t) &= \mathfrak{c}_0 + \frac{(1-\varsigma)\vartheta t^{\vartheta-1}}{\Delta(\varsigma)}\psi_5(t,\mathfrak{s},\mathfrak{i},\mathfrak{l},\mathfrak{u},\mathfrak{c}) + \frac{\varsigma\vartheta}{\Delta(\varsigma)\Gamma(\varsigma)}\int_0^t v^{\vartheta-1}(t-v)^{\varsigma-1}\psi_5(v,\mathfrak{s},\mathfrak{i},\mathfrak{l},\mathfrak{u},\mathfrak{c})dv
\end{aligned}$$

The system (9) & its above solution generalized as follows:

$$\begin{aligned}
{}^{\varsigma}\mathfrak{D}(\mathcal{M}(t)) &= \vartheta t^{\vartheta-1}\Upsilon(t,\mathcal{M}(t))\\
\mathcal{M}(0) &= \mathcal{M}_0
\end{aligned} \tag{10}$$

$$\mathcal{M}(t) = \mathcal{M}_0 + \frac{(1-\varsigma)\vartheta t^{\vartheta-1}}{\Delta(\varsigma)}\Upsilon(t,\mathcal{M}(t)) + \frac{\varsigma\vartheta}{\Delta(\varsigma)\Gamma(\varsigma)}\int_0^t v^{\vartheta-1}(t-v)^{\varsigma-1}\Upsilon(v,\mathcal{M}(v))dv \tag{11}$$

where $\mathcal{M}(t) = \begin{pmatrix}\mathfrak{s}\\ \mathfrak{i}\\ \mathfrak{l}\\ \mathfrak{u}\\ \mathfrak{c}\end{pmatrix}$, the initial condition $\mathcal{M}_0 = \begin{pmatrix}\mathfrak{s}_0\\ \mathfrak{i}_0\\ \mathfrak{l}_0\\ \mathfrak{u}_0\\ \mathfrak{c}_0\end{pmatrix}$,

and the real-valued continuous function $\Upsilon(t,\mathcal{M}(t)) = \begin{pmatrix}\psi_1(t,\mathfrak{s},\mathfrak{i},\mathfrak{l},\mathfrak{u},\mathfrak{c})\\ \psi_2(t,\mathfrak{s},\mathfrak{i},\mathfrak{l},\mathfrak{u},\mathfrak{c})\\ \psi_3(t,\mathfrak{s},\mathfrak{i},\mathfrak{l},\mathfrak{u},\mathfrak{c})\\ \psi_4(t,\mathfrak{s},\mathfrak{i},\mathfrak{l},\mathfrak{u},\mathfrak{c})\\ \psi_5(t,\mathfrak{s},\mathfrak{i},\mathfrak{l},\mathfrak{u},\mathfrak{c})\end{pmatrix}$.

In order to prove the existence of the solution (7) by Schaefer's fixed point theorem, first we define an operator $\Theta : \Omega \to \Omega$ as

$$\Theta(\mathcal{M}(\mathrm{t})) = \mathcal{M}_0 + \frac{(1-\varsigma)\vartheta \mathrm{t}^{\vartheta-1}}{\Delta(\varsigma)}\Upsilon(\mathrm{t},\mathcal{M}) + \frac{\varsigma\vartheta}{\Delta(\varsigma)\Gamma(\varsigma)}\int_0^{\mathrm{t}} \mathrm{v}^{\vartheta-1}(\mathrm{t}-\mathrm{v})^{\varsigma-1}\Upsilon(\mathrm{v},\mathcal{M})d\mathrm{v}$$

Theorem 4.1. [Schaefer's fixed point theorem] *If* $\kappa(\Theta) = \left\{\mathcal{M} \in \Omega \mid \mathcal{M} = \alpha\Theta(\mathcal{M}),\ 0 \le \alpha \le 1\right\}$ *is a bounded set and the operator* Θ *is completely continuous, then* Θ *has at least one fixed point.*

Proof. [Existence] First, we need to show that $\Upsilon(\mathrm{t},\mathcal{M}(\mathrm{t}))$ satisfies the Lipschitz condition.
Let $\mathcal{M},\mathcal{N} \in \Omega$.

(*i*) For two functions $\mathfrak{s}_1$ and $\mathfrak{s}_2$,

$$\begin{aligned}\left|\psi_1(\mathrm{t},\mathfrak{s}_1,\mathfrak{i},\mathfrak{l},\mathfrak{u},\mathfrak{c}) - \psi_1(\mathrm{t},\mathfrak{s}_2,\mathfrak{i},\mathfrak{l},\mathfrak{u},\mathfrak{c})\right| &\le \Big|\tau^{\epsilon} + \delta_1^{\epsilon}(1-\mathfrak{s}_1-\mathfrak{i}) - ({}^{*}\lambda^{\epsilon}+\tau^{\epsilon})\mathfrak{s}_1 \\ &\quad - \tau^{\epsilon} - \delta_1^{\epsilon}(1-\mathfrak{s}_2-\mathfrak{i}) + ({}^{*}\lambda^{\epsilon}+\tau^{\epsilon})\mathfrak{s}_2\Big| \\ &\le \left|\delta_1^{\epsilon} +^{*} \lambda^{\epsilon}+\tau^{\epsilon}\right|\left|\mathfrak{s}_1-\mathfrak{s}_2\right|\end{aligned}$$

Assuming $\mathcal{G}^s_{\psi_1} = \left|\delta_1^{\epsilon} +^{*} \lambda^{\epsilon}+\tau^{\epsilon}\right|$,

$$\left|\psi_1(\mathrm{t},\mathfrak{s}_1,\mathfrak{i},\mathfrak{l},\mathfrak{u},\mathfrak{c}) - \psi_1(\mathrm{t},\mathfrak{s}_2,\mathfrak{i},\mathfrak{l},\mathfrak{u},\mathfrak{c})\right| \le \mathcal{G}^s_{\psi_1}\left|\mathfrak{s}_1-\mathfrak{s}_2\right|$$

In a similar way, for two functions $\mathfrak{i}_1$ and $\mathfrak{i}_2$,

$$\left|\psi_1(\mathrm{t},\mathfrak{s},\mathfrak{i}_1,\mathfrak{l},\mathfrak{u},\mathfrak{c}) - \psi_1(\mathrm{t},\mathfrak{s},\mathfrak{i}_2,\mathfrak{l},\mathfrak{u},\mathfrak{c})\right| \le \mathcal{G}^i_{\psi_1}\left|\mathfrak{i}_1-\mathfrak{i}_2\right|$$

such that $\mathcal{G}^i_{\psi_1} = \left|\delta_1^{\epsilon}\right|$.
Then ψ_1 satisfies the Lipschitz condition for all dependent parameters $\mathfrak{s}$ & $\mathfrak{i}$.

$$\therefore \left|\psi_1(\mathrm{t},\mathcal{M}(\mathrm{t})) - \psi_1(\mathrm{t},\mathcal{N}(\mathrm{t}))\right| \le \mathcal{G}_{\psi_1}\left|\mathcal{M}(\mathrm{t})-\mathcal{N}(\mathrm{t})\right|$$

with $\mathcal{G}_{\psi_1} = \max\left\{\mathcal{G}^s_{\psi_1}, \mathcal{G}^i_{\psi_1}\right\}$

(*ii*) Similarly, we obtain $\mathcal{G}^i_{\psi_2} = \left|\delta_2^{\epsilon}\right|$ and $\mathcal{G}^s_{\psi_2} = \left|{}^{*}\lambda^{\epsilon}\right|$ for ψ_2.
Then with constant $\mathcal{G}_{\psi_2} = \max\left\{\mathcal{G}^i_{\psi_2}, \mathcal{G}^s_{\psi_2}\right\}$,

$$\therefore \left|\psi_2(\mathrm{t},\mathcal{M}(\mathrm{t})) - \psi_2(\mathrm{t},\mathcal{N}(\mathrm{t}))\right| \le \mathcal{G}_{\psi_2}\left|\mathcal{M}(\mathrm{t})-\mathcal{N}(\mathrm{t})\right|$$

(*iii*) Since $0 \le \mathfrak{l} \le 1$, then for ψ_3, $\mathcal{G}^l_{\psi_3} = \left|\sigma^{\epsilon}\right|$ and $\mathcal{G}^l_{\psi_3} = \mathcal{G}_{\psi_3}$.
we obtain

$$\therefore \left|\psi_3(\mathrm{t},\mathcal{M}(\mathrm{t})) - \psi_3(\mathrm{t},\mathcal{N}(\mathrm{t}))\right| \le \mathcal{G}_{\psi_3}\left|\mathcal{M}(\mathrm{t})-\mathcal{N}(\mathrm{t})\right|$$

(*iv*) For ψ_4, $\mathcal{G}^u_{\psi_4} = \left|\mu^{\epsilon} + ({}^{*}\eta)^{\epsilon}\right|$ and $\mathcal{G}^u_{\psi_4} = \mathcal{G}_{\psi_4}$.

$$\therefore \left|\psi_4(\mathrm{t},\mathcal{M}(\mathrm{t})) - \psi_4(\mathrm{t},\mathcal{N}(\mathrm{t}))\right| \le \mathcal{G}_{\psi_4}\left|\mathcal{M}(\mathrm{t})-\mathcal{N}(\mathrm{t})\right|$$

(v) In a similar way, we get $\mathcal{G}^u_{\psi_5} = \Big|(^*\eta)^\epsilon\Big|$ and $\mathcal{G}^c_{\psi_5} = \Big|\mu^\epsilon\Big|$

$$\therefore \Big|\psi_5(\mathrm{t},\mathcal{M}(\mathrm{t})) - \psi_5(\mathrm{t},\mathcal{N}(\mathrm{t}))\Big| \leq \mathcal{G}_{\psi_5}\Big|\mathcal{M}(\mathrm{t}) - \mathcal{N}(\mathrm{t})\Big|$$

where $\mathcal{G}_{\psi_5} = \max\Big\{\mathcal{G}^u_{\psi_2}, \mathcal{G}^c_{\psi_2}\Big\}$.

Since all $\psi_1, \psi_2, \psi_3, \psi_4, \psi_5$ satisfies the Lipschitz condition.
Then by considering $\mathcal{G}_\Upsilon = \max\Big\{\mathcal{G}_{\psi_1}, \mathcal{G}_{\psi_2}, \mathcal{G}_{\psi_3}, \mathcal{G}_{\psi_4}, \mathcal{G}_{\psi_5}\Big\}$, we can achieve that for $\mathcal{M}, \mathcal{N} \in \Omega$

$$\Big|\Upsilon(\mathrm{t},\mathcal{M}(\mathrm{t})) - \Upsilon(\mathrm{t},\mathcal{N}(\mathrm{t}))\Big| \leq \mathcal{G}_\Upsilon\Big|\mathcal{M}(\mathrm{t}) - \mathcal{N}(\mathrm{t})\Big| \tag{12}$$

Hence, $\Upsilon(\mathrm{t},\mathcal{M})$ satisfies the Lipschitz condition.
In order to prove that Θ is continuous, assume that a sequence of $\{\mathcal{M}_\mathrm{k}\}$ converges to $\mathcal{M}$ in Ω.

$$\Big\|\Theta\Big(\mathcal{M}_\mathrm{k}\Big) - \Theta\Big(\mathcal{M}\Big)\Big\| \leq \max_{\mathrm{t}\in I}\Bigg(\frac{(1-\varsigma)\vartheta \mathrm{t}^{\vartheta-1}}{\Delta(\varsigma)}\Big|\Upsilon(\mathrm{t},\mathcal{M}_\mathrm{k}(\mathrm{t})) - \Upsilon(\mathrm{t},\mathcal{M}(\mathrm{t}))\Big|$$
$$+ \frac{\varsigma\vartheta}{\Delta(\varsigma)\Gamma(\varsigma)}\int_0^\mathrm{t} \mathrm{v}^{\vartheta-1}(\mathrm{t}-\mathrm{v})^{\varsigma-1}\Big|\Upsilon(\mathrm{v},\mathcal{M}_\mathrm{k}(\mathrm{v})) - \Upsilon(\mathrm{v},\mathcal{M}(\mathrm{v}))\Big|d\mathrm{v}\Bigg)$$

$$\leq \frac{(1-\varsigma)\vartheta\, T^{\vartheta-1}}{\Delta(\varsigma)}\mathcal{G}_\Upsilon\,\|\mathcal{M}_\mathrm{k} - \mathcal{M}\| + \frac{\varsigma\vartheta}{\Delta(\varsigma)\Gamma(\varsigma)}\mathcal{G}_\Upsilon\,\|\mathcal{M}_\mathrm{k} - \mathcal{M}\|\max_{\mathrm{t}\in I}\int_0^\mathrm{t} \mathrm{v}^{\vartheta-1}(\mathrm{t}-\mathrm{v})^{\varsigma-1}d\mathrm{v}$$

After taking $\mathrm{v} = \mathrm{tw}$, we achieved $\int_0^\mathrm{t} \mathrm{v}^{\vartheta-1}(\mathrm{t}-\mathrm{v})^{\varsigma-1}d\mathrm{v} = \int_0^1 \mathrm{t}^\epsilon \mathrm{w}^{\vartheta-1}(1-\mathrm{w})^{\varsigma-1}d\mathrm{w}$
Substituding the above integral and Beta function $\mathcal{B}(\varsigma,\vartheta)$, we obtain

$$\Big\|\Theta\Big(\mathcal{M}_\mathrm{k}\Big) - \Theta\Big(\mathcal{M}\Big)\Big\| \leq \left[\frac{(1-\varsigma)\vartheta\, T^{\vartheta-1}}{\Delta(\varsigma)} + \frac{\varsigma\vartheta\, T^\epsilon}{\Delta(\varsigma)\Gamma(\varsigma)}\mathcal{B}(\varsigma,\vartheta)\right]\mathcal{G}_\Upsilon\,\|\mathcal{M}_\mathrm{k} - \mathcal{M}\|$$

$$\Big\|\Theta\Big(\mathcal{M}_\mathrm{k}\Big) - \Theta\Big(\mathcal{M}\Big)\Big\| \leq \Xi\mathcal{G}_\Upsilon\,\|\mathcal{M}_\mathrm{k} - \mathcal{M}\| \tag{13}$$

where $\Xi = \left[\frac{(1-\varsigma)\vartheta\, T^{\vartheta-1}}{\Delta(\varsigma)} + \frac{\varsigma\vartheta\, T^\epsilon}{\Delta(\varsigma)\Gamma(\varsigma)}\mathcal{B}(\varsigma,\vartheta)\right]$.
Hence $\Theta\Big(\mathcal{M}_\mathrm{k}\Big) \to \Theta\Big(\mathcal{M}\Big)$ whenever $\{\mathcal{M}_\mathrm{k}\} \to \mathcal{M}$ as k tends to ∞.
$\therefore \Theta$ is continuous.
Now, for a bounded set $\mathcal{M}$ of Ω, there is a bound $\mathcal{A}_\Upsilon$.
For all $\mathcal{M}$, $\Big\|\Theta\Big(\mathcal{M}\Big)\Big\| \leq \Xi\ \mathcal{A}_\Upsilon$.
$\therefore \Theta$ is uniformly bounded.
For $\mathrm{t}, \mathrm{w} \in I$,

$$\Big\|\Theta\Big(\mathcal{M}(\mathrm{t})\Big) - \Theta\Big(\mathcal{M}(\mathrm{w})\Big)\Big\| \leq \left[\frac{(1-\varsigma)\vartheta}{\Delta(\varsigma)}\mathcal{A}_\Upsilon\right](\mathrm{t}^{\vartheta-1} - \mathrm{w}^{\vartheta-1})$$
$$+ \left[\left[\frac{(1-\varsigma)\vartheta\, T^{\vartheta-1}}{\Delta(\varsigma)} + \frac{\varsigma\vartheta\mathcal{A}_\Upsilon}{\Delta(\varsigma)\Gamma(\varsigma)}\mathcal{B}(\varsigma,\vartheta)\right](\mathrm{t}^\epsilon - \mathrm{w}^\epsilon)\right.$$

$\therefore \left\|\Theta\Big(\mathcal{M}(\mathrm{t})\Big) - \Theta\Big(\mathcal{M}(\mathrm{w})\Big)\right\| \to 0$ as $\mathrm{t} \to \mathrm{w}$. Then, Θ is uniformly continuous.
From the Arzela-Ascoli theorem, Θ is equicontinuous and relatively compact.
$\therefore \Theta$ is completely continuous.
Let $\mathcal{N} \in \kappa$. Then $\|\mathcal{N}\| = \|\alpha\Theta(\mathcal{M})\| \leq \Xi\ \mathcal{A}_{\Upsilon}$.
Hence, κ is bounded, and from Theorem 4.1, Θ has at least one fixed point. □

Theorem 4.2. [Uniqueness] *If $\Xi\mathcal{G}_{\Upsilon} < 1$, then system (7) has a unique solution.*

Proof. Let $\mathcal{X}_{\mathcal{M}} = \max_{\mathrm{t}\in I} |\Upsilon(\mathrm{t}, 0)| < \infty$ such that $\Xi(\mathcal{G}_{\Upsilon} Y + \mathcal{X}_{\mathcal{M}}) \leq Y$.
Assume that $\mathcal{Z}_Y = \{\mathcal{M} \in \Omega : \|\mathcal{M}\| \leq Y\}$ and we need to prove that $\Theta(\mathcal{Z}_Y) \subset \mathcal{Z}_Y$.

$$\|\Theta(\mathcal{M})\| \leq \max_{\mathrm{t}\in I}\Bigg(\frac{(1-\varsigma)\vartheta \mathrm{t}^{\vartheta-1}}{\Delta(\varsigma)}\Big[\Big|\Upsilon\big(\mathrm{t}, \mathcal{M}(\mathrm{t})\big) - \Upsilon(\mathrm{t}, 0)\Big| + \Big|\Upsilon(\mathrm{t}, 0)\Big|\Big] + \frac{\varsigma\vartheta}{\Delta(\varsigma)\Gamma(\varsigma)}\int_0^{\mathrm{t}} \mathrm{v}^{\vartheta-1}(\mathrm{t}-\mathrm{v})^{\varsigma-1}\Big[\Big|\Upsilon\big(\mathrm{t}, \mathcal{M}(\mathrm{t})\big) - \Upsilon(\mathrm{t}, 0)\Big| + \Big|\Upsilon(\mathrm{t}, 0)\Big|\Big]d\mathrm{v}\Bigg)$$

$$\begin{aligned}\therefore \|\Theta(\mathcal{M})\| &\leq \Xi(\mathcal{G}_{\Upsilon}\|\mathcal{M}\| + \mathcal{X}_{\mathcal{M}}) \\ &\leq \Xi(\mathcal{G}_{\Upsilon} Y + \mathcal{X}_{\mathcal{M}}) \\ &\leq Y\end{aligned}$$

Hence $\|\Theta(\mathcal{M})\| \leq \mathrm{Y}$, $\forall\ \mathcal{M} \in \mathcal{Z}_Y$.
For every $\mathcal{M}, \mathcal{N} \in \Omega$ and each $\mathrm{t} \in I$, we achieve $\|\Theta(\mathcal{M}) - \Theta(\mathcal{N})\| \leq \Xi\mathcal{G}_{\Upsilon}\ \|\mathcal{M} - \mathcal{N}\|$
Since $\Xi\mathcal{G}_{\Upsilon} < 1$, then the operator Θ possesses contraction.
Considering the Banach fixed-point theorem, the system (7) has a unique solution. □

5 Ulam-Hyers Stability

The stability of the system (7) is analysed to understand its behaviour over time and ensure its reliability. This examination is essential to determine how the model's solutions react to slight changes in initial conditions or parameter values. The study specifically explores Ulam-Hyers stability, which helps evaluate the robustness of the solutions by confirming that approximate solutions stay close to the exact solution when small deviations occur.
Let us consider a small change perturbed by Φ that depends only on the solution with initial conditions $\Phi(0) = 0$ and $|\Phi(\mathrm{t})| \leq \zeta$.
The system becomes

$$\begin{aligned}{}^{\varsigma}\mathfrak{D}\big(\mathcal{M}(\mathrm{t})\big) &= \vartheta \mathrm{t}^{\vartheta-1}\Upsilon\big(\mathrm{t}, \mathcal{M}(\mathrm{t})\big) + \Phi(\mathrm{t}) \\ \mathcal{M}(0) &= \mathcal{M}_0\end{aligned} \tag{14}$$

Lemma 5.1. *The system (14) satisfies*

$$\left|\mathcal{M}(\mathrm{t}) - \Big(\mathcal{M}_0 + \tfrac{(1-\varsigma)\vartheta \mathrm{t}^{\vartheta-1}}{\Delta(\varsigma)}\Upsilon\big(\mathrm{t}, \mathcal{M}(\mathrm{t})\big) + \tfrac{\varsigma\vartheta}{\Delta(\varsigma)\Gamma(\varsigma)}\int_0^{\mathrm{t}} \mathrm{v}^{\vartheta-1}(\mathrm{t}-\mathrm{v})^{\varsigma-1}\Upsilon\big(\mathrm{v}, \mathcal{M}(\mathrm{v})\big)d\mathrm{v}\Big)\right| \leq (\Xi\zeta). \tag{15}$$

Proof. The equation (11) and $|\Phi(\mathrm{t})| \leq \zeta$ implies the solution (15). □

Theorem 5.2. *If* $(\Xi\mathcal{G}_\Upsilon) < 1$ *and Lemma 5.1 holds, then the system is Ulam-Hyers stable.*

Proof. For $\mathrm{t} \in I$,

$$|\mathcal{M}(\mathrm{t}) - \mathcal{N}(\mathrm{t})| = \left|\mathcal{M}(\mathrm{t}) - \left(\mathcal{N}_0 + \tfrac{(1-\varsigma)\vartheta \mathrm{t}^{\vartheta-1}}{\Delta(\varsigma)}\Upsilon(\mathrm{t},\mathcal{N}(\mathrm{t})) + \tfrac{\varsigma\vartheta}{\Delta(\varsigma)\Gamma(\varsigma)}\int_0^{\mathrm{t}} \mathrm{v}^{\vartheta-1}(\mathrm{t}-\mathrm{v})^{\varsigma-1}\Upsilon(\mathrm{v},\mathcal{N}(\mathrm{v}))d\mathrm{v}\right)\right|$$

$$\begin{aligned}
&\leq \left|\mathcal{M}(\mathrm{t}) - \left(\mathcal{M}_0 + \frac{(1-\varsigma)\vartheta \mathrm{t}^{\vartheta-1}}{\Delta(\varsigma)}\Upsilon(\mathrm{t},\mathcal{M}(\mathrm{t})) + \frac{\varsigma\vartheta}{\Delta(\varsigma)\Gamma(\varsigma)}\int_0^{\mathrm{t}} \mathrm{v}^{\vartheta-1}(\mathrm{t}-\mathrm{v})^{\varsigma-1}\Upsilon(\mathrm{v},\mathcal{M}(\mathrm{v}))d\mathrm{v}\right)\right| \\
&\quad + \left|\left(\mathcal{M}_0 + \frac{(1-\varsigma)\vartheta \mathrm{t}^{\vartheta-1}}{\Delta(\varsigma)}\Upsilon(\mathrm{t},\mathcal{M}(\mathrm{t})) + \frac{\varsigma\vartheta}{\Delta(\varsigma)\Gamma(\varsigma)}\int_0^{\mathrm{t}} \mathrm{v}^{\vartheta-1}(\mathrm{t}-\mathrm{v})^{\varsigma-1}\Upsilon(\mathrm{v},\mathcal{M}(\mathrm{v}))d\mathrm{v}\right)\right. \\
&\quad \left. - \left(\mathcal{N}_0 + \frac{(1-\varsigma)\vartheta \mathrm{t}^{\vartheta-1}}{\Delta(\varsigma)}\Upsilon(\mathrm{t},\mathcal{N}(\mathrm{t})) + \frac{\varsigma\vartheta}{\Delta(\varsigma)\Gamma(\varsigma)}\int_0^{\mathrm{t}} \mathrm{v}^{\vartheta-1}(\mathrm{t}-\mathrm{v})^{\varsigma-1}\Upsilon(\mathrm{v},\mathcal{N}(\mathrm{v}))d\mathrm{v}\right)\right|
\end{aligned}$$

$$\leq (\Xi\zeta) + (\Xi\mathcal{G}_\Upsilon)\,\|\mathcal{M}-\mathcal{N}\|$$

$$\therefore \|\mathcal{M}-\mathcal{N}\| \leq \left(\frac{\Xi}{1-(\Xi\mathcal{G}_\Upsilon)}\right)\zeta = \mathfrak{C}\zeta$$

Hence, the system is Ulam-Hyers stable. □

6 Computational Analysis

In this section, we present a novel numerical scheme to solve the system, and results obtained from the MATLAB simulations of the Listeriosis disease model are illustrated.
The solution of the system (7) is given by

$$\begin{aligned}
\mathfrak{s}(\mathrm{t}) &= \mathfrak{s}_0 + \frac{(1-\varsigma)\vartheta \mathrm{t}^{\vartheta-1}}{\Delta(\varsigma)}\psi_1(\mathrm{t},\mathfrak{s},\mathfrak{i},\mathfrak{l},\mathfrak{u},\mathfrak{c}) + \frac{\varsigma\vartheta}{\Delta(\varsigma)\Gamma(\varsigma)}\int_0^{\mathrm{t}} \mathrm{v}^{\vartheta-1}(\mathrm{t}-\mathrm{v})^{\varsigma-1}\psi_1(\mathrm{v},\mathfrak{s},\mathfrak{i},\mathfrak{l},\mathfrak{u},\mathfrak{c})d\mathrm{v} \\
\mathfrak{i}(\mathrm{t}) &= \mathfrak{i}_0 + \frac{(1-\varsigma)\vartheta \mathrm{t}^{\vartheta-1}}{\Delta(\varsigma)}\psi_2(\mathrm{t},\mathfrak{s},\mathfrak{i},\mathfrak{l},\mathfrak{u},\mathfrak{c}) + \frac{\varsigma\vartheta}{\Delta(\varsigma)\Gamma(\varsigma)}\int_0^{\mathrm{t}} \mathrm{v}^{\vartheta-1}(\mathrm{t}-\mathrm{v})^{\varsigma-1}\psi_2(\mathrm{v},\mathfrak{s},\mathfrak{i},\mathfrak{l},\mathfrak{u},\mathfrak{c})d\mathrm{v} \\
\mathfrak{l}(\mathrm{t}) &= \mathfrak{l}_0 + \frac{(1-\varsigma)\vartheta \mathrm{t}^{\vartheta-1}}{\Delta(\varsigma)}\psi_3(\mathrm{t},\mathfrak{s},\mathfrak{i},\mathfrak{l},\mathfrak{u},\mathfrak{c}) + \frac{\varsigma\vartheta}{\Delta(\varsigma)\Gamma(\varsigma)}\int_0^{\mathrm{t}} \mathrm{v}^{\vartheta-1}(\mathrm{t}-\mathrm{v})^{\varsigma-1}\psi_3(\mathrm{v},\mathfrak{s},\mathfrak{i},\mathfrak{l},\mathfrak{u},\mathfrak{c})d\mathrm{v} \\
\mathfrak{u}(\mathrm{t}) &= \mathfrak{u}_0 + \frac{(1-\varsigma)\vartheta \mathrm{t}^{\vartheta-1}}{\Delta(\varsigma)}\psi_4(\mathrm{t},\mathfrak{s},\mathfrak{i},\mathfrak{l},\mathfrak{u},\mathfrak{c}) + \frac{\varsigma\vartheta}{\Delta(\varsigma)\Gamma(\varsigma)}\int_0^{\mathrm{t}} \mathrm{v}^{\vartheta-1}(\mathrm{t}-\mathrm{v})^{\varsigma-1}\psi_4(\mathrm{v},\mathfrak{s},\mathfrak{i},\mathfrak{l},\mathfrak{u},\mathfrak{c})d\mathrm{v} \\
\mathfrak{c}(\mathrm{t}) &= \mathfrak{c}_0 + \frac{(1-\varsigma)\vartheta \mathrm{t}^{\vartheta-1}}{\Delta(\varsigma)}\psi_5(\mathrm{t},\mathfrak{s},\mathfrak{i},\mathfrak{l},\mathfrak{u},\mathfrak{c}) + \frac{\varsigma\vartheta}{\Delta(\varsigma)\Gamma(\varsigma)}\int_0^{\mathrm{t}} \mathrm{v}^{\vartheta-1}(\mathrm{t}-\mathrm{v})^{\varsigma-1}\psi_5(\mathrm{v},\mathfrak{s},\mathfrak{i},\mathfrak{l},\mathfrak{u},\mathfrak{c})d\mathrm{v}
\end{aligned}$$

Taking a 'j' partition with a difference b on the integral limits,

$$\mathfrak{s}(\mathrm{t_{j+1}}) = \mathfrak{s}_0 + \frac{(1-\varsigma)\vartheta \mathrm{t_j}^{\vartheta-1}}{\Delta(\varsigma)}\psi_1(\mathrm{t_j},\mathfrak{s},\mathfrak{i},\mathfrak{l},\mathfrak{u},\mathfrak{c}) + \frac{\varsigma\vartheta}{\Delta(\varsigma)\Gamma(\varsigma)}\sum_{n=0}^{\mathrm{j}}\int_{\mathrm{t}_n}^{\mathrm{t}_{n+1}} \mathrm{v}^{\vartheta-1}(\mathrm{t_{j+1}}-\mathrm{v})^{\varsigma-1}\psi_1(\mathrm{v},\mathfrak{s},\mathfrak{i},\mathfrak{l},\mathfrak{u},\mathfrak{c})d\mathrm{v}$$

$$\mathfrak{i}(\mathrm{t_{j+1}}) = \mathfrak{i}_0 + \frac{(1-\varsigma)\vartheta \mathrm{t_j}^{\vartheta-1}}{\Delta(\varsigma)}\psi_2(\mathrm{t_j},\mathfrak{s},\mathfrak{i},\mathfrak{l},\mathfrak{u},\mathfrak{c}) + \frac{\varsigma\vartheta}{\Delta(\varsigma)\Gamma(\varsigma)}\sum_{n=0}^{\mathrm{j}}\int_{\mathrm{t}_n}^{\mathrm{t}_{n+1}} \mathrm{v}^{\vartheta-1}(\mathrm{t_{j+1}}-\mathrm{v})^{\varsigma-1}\psi_2(\mathrm{v},\mathfrak{s},\mathfrak{i},\mathfrak{l},\mathfrak{u},\mathfrak{c})d\mathrm{v}$$

$$\mathfrak{l}(\mathrm{t_{j+1}}) = \mathfrak{l}_0 + \frac{(1-\varsigma)\vartheta \mathrm{t_j}^{\vartheta-1}}{\Delta(\varsigma)}\psi_3(\mathrm{t_j},\mathfrak{s},\mathfrak{i},\mathfrak{l},\mathfrak{u},\mathfrak{c}) + \frac{\varsigma\vartheta}{\Delta(\varsigma)\Gamma(\varsigma)}\sum_{n=0}^{\mathrm{j}}\int_{\mathrm{t}_n}^{\mathrm{t}_{n+1}} \mathrm{v}^{\vartheta-1}(\mathrm{t_{j+1}}-\mathrm{v})^{\varsigma-1}\psi_3(\mathrm{v},\mathfrak{s},\mathfrak{i},\mathfrak{l},\mathfrak{u},\mathfrak{c})d\mathrm{v}$$

$$\mathfrak{u}(\mathrm{t_{j+1}}) = \mathfrak{u}_0 + \frac{(1-\varsigma)\vartheta \mathrm{t_j}^{\vartheta-1}}{\Delta(\varsigma)}\psi_4(\mathrm{t_j},\mathfrak{s},\mathfrak{i},\mathfrak{l},\mathfrak{u},\mathfrak{c}) + \frac{\varsigma\vartheta}{\Delta(\varsigma)\Gamma(\varsigma)}\sum_{n=0}^{\mathrm{j}}\int_{\mathrm{t}_n}^{\mathrm{t}_{n+1}} \mathrm{v}^{\vartheta-1}(\mathrm{t_{j+1}}-\mathrm{v})^{\varsigma-1}\psi_4(\mathrm{v},\mathfrak{s},\mathfrak{i},\mathfrak{l},\mathfrak{u},\mathfrak{c})d\mathrm{v}$$

$$\mathfrak{c}(\mathrm{t_{j+1}}) = \mathfrak{c}_0 + \frac{(1-\varsigma)\vartheta \mathrm{t_j}^{\vartheta-1}}{\Delta(\varsigma)}\psi_5(\mathrm{t_j},\mathfrak{s},\mathfrak{i},\mathfrak{l},\mathfrak{u},\mathfrak{c}) + \frac{\varsigma\vartheta}{\Delta(\varsigma)\Gamma(\varsigma)}\sum_{n=0}^{\mathrm{j}}\int_{\mathrm{t}_n}^{\mathrm{t}_{n+1}} \mathrm{v}^{\vartheta-1}(\mathrm{t_{j+1}}-\mathrm{v})^{\varsigma-1}\psi_5(\mathrm{v},\mathfrak{s},\mathfrak{i},\mathfrak{l},\mathfrak{u},\mathfrak{c})d\mathrm{v}$$

We derived our results by substituting the Lagrange piece-wise interpolation [29] into the computational framework and then performing basic integrals, which led us to obtain the following results:

$$\begin{aligned}
\mathfrak{s}(\mathrm{t_{j+1}}) &= \mathfrak{s}_0 + \frac{(1-\varsigma)\vartheta \mathrm{t_j}^{\vartheta-1}}{\Delta(\varsigma)}\psi_1(\mathrm{t_j},\mathfrak{s},\mathfrak{i},\mathfrak{l},\mathfrak{u},\mathfrak{c}) + \frac{\vartheta b^{\varsigma}}{\Delta(\varsigma)\Gamma(\varsigma+2)} \\
&\quad\times\sum_{n=0}^{\mathrm{j}}\Bigg[\mathrm{t}_n^{\vartheta-1}\psi_1(\mathrm{t}_n,\mathfrak{s},\mathfrak{i},\mathfrak{l},\mathfrak{u},\mathfrak{c})\Big((\mathrm{j}+1-n)^{\varsigma}(\mathrm{j}-n+2+\varsigma)-(\mathrm{j}-n)^{\varsigma}(\mathrm{j}-n+2+2\varsigma)\Big) \\
&\quad-\mathrm{t}_{n-1}^{\vartheta-1}\psi_1(\mathrm{t}_{n-1},\mathfrak{s},\mathfrak{i},\mathfrak{l},\mathfrak{u},\mathfrak{c})\Big((\mathrm{j}-n+1)^{\varsigma+1}-(\mathrm{j}-n)^{\varsigma}(\mathrm{j}-n+1+\varsigma)\Big)\Bigg] \\
\mathfrak{i}(t_{j+1}) &= \mathfrak{i}_0 + \frac{(1-\varsigma)\vartheta \mathrm{t_j}^{\vartheta-1}}{\Delta(\varsigma)}\psi_2(\mathrm{t_j},\mathfrak{s},\mathfrak{i},\mathfrak{l},\mathfrak{u},\mathfrak{c}) + \frac{\vartheta b^{\vartheta}}{\Delta(\varsigma)\Gamma(\varsigma+2)} \\
&\quad\times\sum_{n=0}^{\mathrm{j}}\Bigg[\mathrm{t}_n^{\vartheta-1}\psi_2(\mathrm{t}_n,\mathfrak{s},\mathfrak{i},\mathfrak{l},\mathfrak{u},\mathfrak{c})\Big((\mathrm{j}+1-n)^{\varsigma}(\mathrm{j}-n+2+\varsigma)-(\mathrm{j}-n)^{\varsigma}(\mathrm{j}-n+2+2\varsigma)\Big) \\
&\quad-\mathrm{t}_{n-1}^{\vartheta-1}\psi_2(\mathrm{t}_{n-1},\mathfrak{s},\mathfrak{i},\mathfrak{l},\mathfrak{u},\mathfrak{c})\Big((\mathrm{j}-n+1)^{\varsigma+1}-(\mathrm{j}-n)^{\varsigma}(\mathrm{j}-n+1+\varsigma)\Big)\Bigg]
\end{aligned}$$

$$
\begin{aligned}
\mathfrak{l}(\mathrm{t}_{\mathrm{j}+1}) &= \mathfrak{l}_0 + \frac{(1-\varsigma)\vartheta \mathrm{t}_{\mathrm{j}}^{\vartheta-1}}{\Delta(\varsigma)}\psi_3(\mathrm{t}_{\mathrm{j}}, \mathfrak{s}, \mathfrak{i}, \mathfrak{l}, \mathfrak{u}, \mathfrak{c}) + \frac{\vartheta b^{\varsigma}}{\Delta(\varsigma)\Gamma(\varsigma+2)} \\
&\quad \times \sum_{n=0}^{\mathrm{j}} \Bigg[\mathrm{t}_n^{\vartheta-1}\psi_3(\mathrm{t}_n, \mathfrak{s}, \mathfrak{i}, \mathfrak{l}, \mathfrak{u}, \mathfrak{c}) \Big((\mathrm{j}+1-n)^{\varsigma}(\mathrm{j}-n+2+\varsigma) - (\mathrm{j}-n)^{\varsigma}(\mathrm{j}-n+2+2\varsigma) \Big) \\
&\quad - \mathrm{t}_{n-1}^{\vartheta-1}\psi_3(\mathrm{t}_{n-1}, \mathfrak{s}, \mathfrak{i}, \mathfrak{l}, \mathfrak{u}, \mathfrak{c}) \Big((\mathrm{j}-n+1)^{\varsigma+1} - (\mathrm{j}-n)^{\varsigma}(\mathrm{j}-n+1+\varsigma) \Big) \Bigg] \\
\mathfrak{u}(\mathrm{t}_{\mathrm{j}+1}) &= \mathfrak{u}_0 + \frac{(1-\varsigma)\vartheta \mathrm{t}_{\mathrm{j}}^{\vartheta-1}}{\Delta(\varsigma)}\psi_4(\mathrm{t}_{\mathrm{j}}, \mathfrak{s}, \mathfrak{i}, \mathfrak{l}, \mathfrak{u}, \mathfrak{c}) + \frac{\vartheta b^{\varsigma}}{\Delta(\varsigma)\Gamma(\varsigma+2)} \\
&\quad \times \sum_{n=0}^{\mathrm{j}} \Bigg[\mathrm{t}_n^{\vartheta-1}\psi_4(\mathrm{t}_n, \mathfrak{s}, \mathfrak{i}, \mathfrak{l}, \mathfrak{u}, \mathfrak{c}) \Big((\mathrm{j}+1-n)^{\varsigma}(\mathrm{j}-n+2+\varsigma) - (\mathrm{j}-n)^{\varsigma}(\mathrm{j}-n+2+2\varsigma) \Big) \\
&\quad - \mathrm{t}_{n-1}^{\vartheta-1}\psi_4(\mathrm{t}_{n-1}, \mathfrak{s}, \mathfrak{i}, \mathfrak{l}, \mathfrak{u}, \mathfrak{c}) \Big((\mathrm{j}-n+1)^{\varsigma+1} - (\mathrm{j}-n)^{\varsigma}(\mathrm{j}-n+1+\varsigma) \Big) \Bigg] \\
\mathfrak{c}(\mathrm{t}_{\mathrm{j}+1}) &= \mathfrak{c}_0 + \frac{(1-\varsigma)\vartheta \mathrm{t}_{\mathrm{j}}^{\vartheta-1}}{\Delta(\varsigma)}\psi_5(\mathrm{t}_{\mathrm{j}}, \mathfrak{s}, \mathfrak{i}, \mathfrak{l}, \mathfrak{u}, \mathfrak{c}) + \frac{\vartheta b^{\varsigma}}{\Delta(\varsigma)\Gamma(\varsigma+2)} \\
&\quad \times \sum_{n=0}^{\mathrm{j}} \Bigg[\mathrm{t}_n^{\vartheta-1}\psi_5(\mathrm{t}_n, \mathfrak{s}, \mathfrak{i}, \mathfrak{l}, \mathfrak{u}, \mathfrak{c}) \Big((\mathrm{j}+1-n)^{\varsigma}(\mathrm{j}-n+2+\varsigma) - (\mathrm{j}-n)^{\varsigma}(\mathrm{j}-n+2+2\varsigma) \Big) \\
&\quad - \mathrm{t}_{n-1}^{\vartheta-1}\psi_5(\mathrm{t}_{n-1}, \mathfrak{s}, \mathfrak{i}, \mathfrak{l}, \mathfrak{u}, \mathfrak{c}) \Big((\mathrm{j}-n+1)^{\varsigma+1} - (\mathrm{j}-n)^{\varsigma}(\mathrm{j}-n+1+\varsigma) \Big) \Bigg]
\end{aligned} \tag{16}
$$

6.1 Fractal-Fractional Model Results

The solution (16) of the Listeriosis disease model has been evaluated through comprehensive MATLAB simulations, utilizing specified initial conditions, $\mathfrak{s}_0 = 0.6$, $\mathfrak{i}_0 = 0.3$, $\mathfrak{l}_0 = 0.45$, $\mathfrak{u}_0 = 0.7$, and $\mathfrak{c}_0 = 0.3$. These values & the Table 1 values are assumed for evaluation. The results obtained from these simulations are systematically analysed and discussed in detail below:

1. Human Population: Graph 2 shows the susceptible, infected, and recovered population over time for different values of ς and ϑ. The results indicate that the susceptible population decreases over time for all parameter values, with slight variations in the rate of decrease depending on the values. The susceptible population 2(a) starts to decrease significantly after approximately 5 units of time. For the infected population, the results 2(b) demonstrate that a marked reduction in the infected population becomes evident around 10 time units. Similarly, the recovered population 2(c) shows an upward trend over time for all values of fractal and fractional. The growth rate varies slightly with different parameter values, with a notable increase occurring after approximately 10 time units.
   Plot 3 indicates how the infected population changes over time as the susceptible population varies and reveals that as the susceptible population decreases, the infected population initially increases and then decreases over time. The plot 4 shows how the recovered population changes over time as the infected population varies and reveals that as the infected population decreases, the recovered population increases over time.

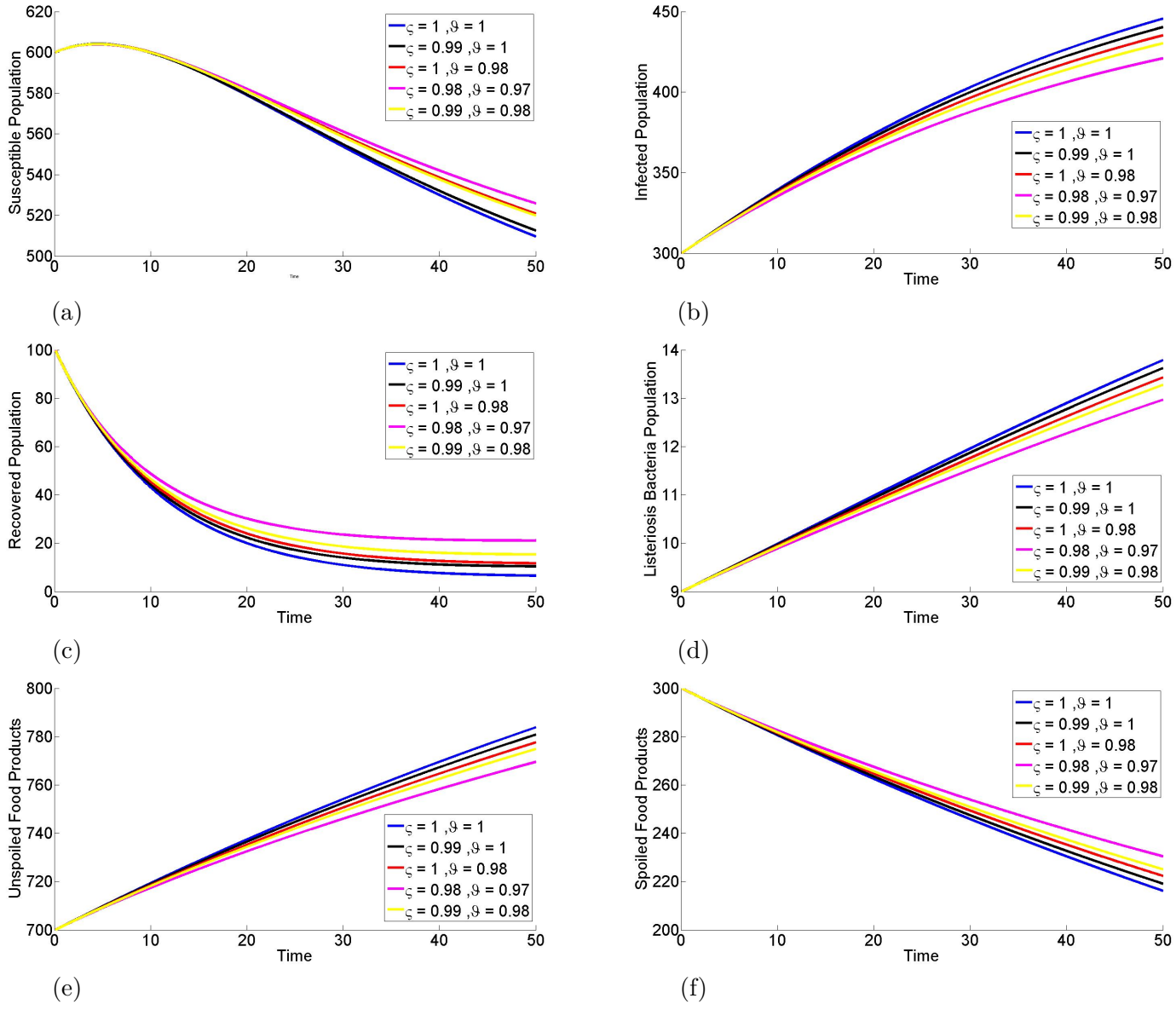

Figure 2: Dynamic behaviour of the populations under varying fractal and fractional values

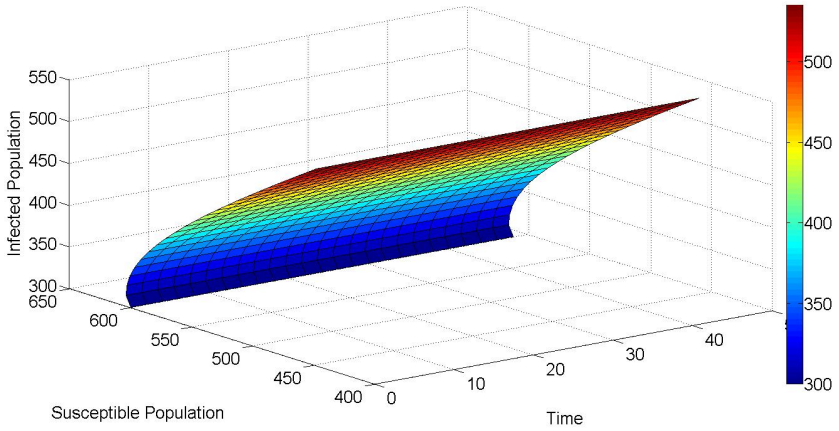

Figure 3: Comparison of the susceptible and infected populations over time

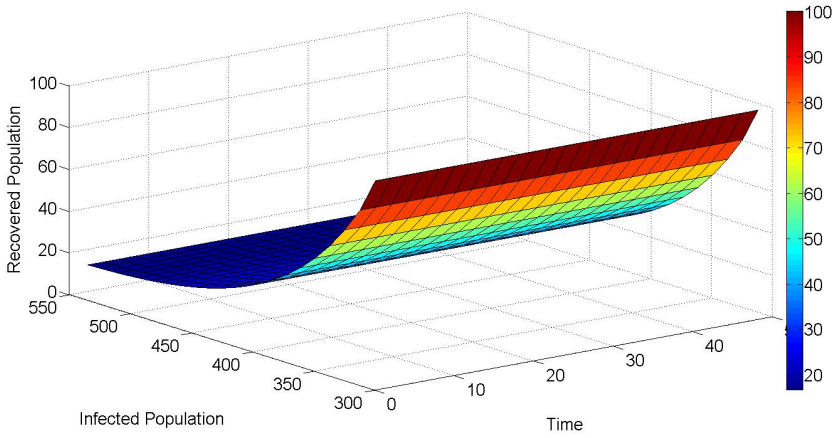

Figure 4: Comparison of the infected and recovered populations over time

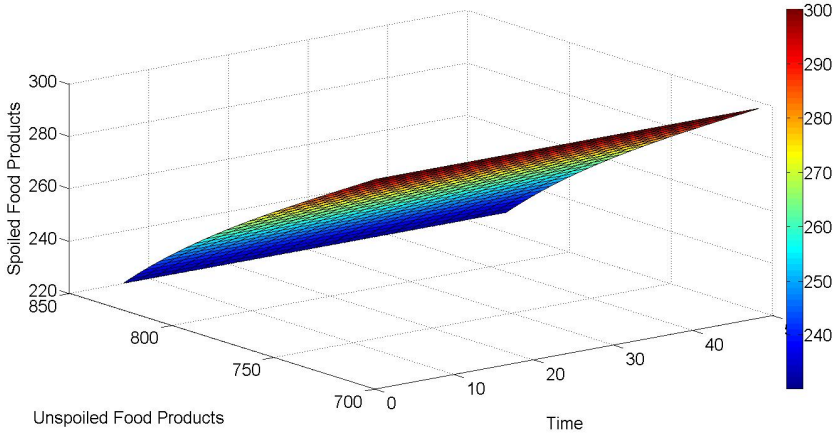

Figure 5: Comparison of the unspoiled and spoiled food production over time

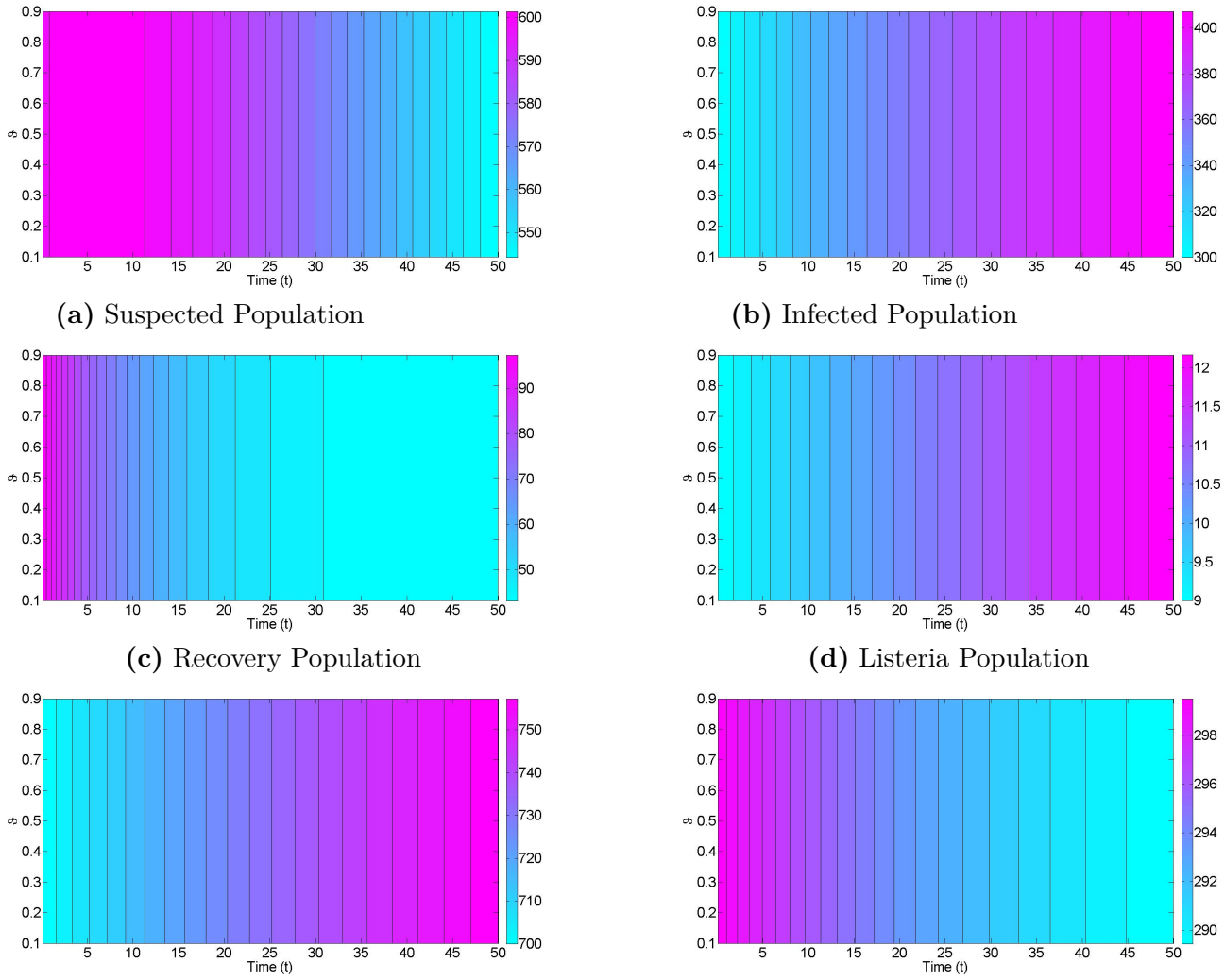

(a) Suspected Population

(b) Infected Population

(c) Recovery Population

(d) Listeria Population

(e) Uncontaminated Food Products

(f) Contaminated Food Products

Figure 6: Impact of Parameter ϑ on Population Dynamics and Food Product Variation

2. Listeriosis Population: Figure 2(d) depicts the population of Listeriosis bacteria over time for various fractal and fractional values. The bacterial population starts to decrease significantly after approximately 5 units of time.

3. Food products: The results 2(e)&(f) show that the number of unspoiled food products starts to decrease significantly after approximately 5 units of time, and there is a significant decrease in the spoiled food products after 5units of time. Plot 5 shows how the number of unspoiled food products changes over time as the spoiled food products vary and reveals that as the spoiled food products decrease, the unspoiled food products increase over time.

These findings demonstrate the effectiveness of our fractal-fractional model in capturing the complex dynamics of Listeriosis disease, providing a more accurate representation of the disease's behaviour and aiding in the development of effective control strategies.

6.2 Significance of Fractal Dimension

Traditional Euclidean geometry assumes a uniform and homogeneous space where interactions, such as disease transmission, occur evenly across the environment. However, real-world environments are far more complex, featuring uneven population distributions and irregular social networks. These complexities include heterogeneous population densities and clustered community structures, which deviate significantly from uniform interaction patterns. The fractal dimension plays a crucial role in modelling systems with uneven population densities and varied infrastructures.

In the context of the SIR model, ϑ sheds light on contact patterns within populations, helping to capture how individuals interact in different environments. Additionally, ϑ can describe bacterial growth patterns, which often follow irregular distributions influenced by environmental conditions. In the realm of food products, ϑ is instrumental in analysing spoilage patterns, revealing how food deterioration may vary spatially and temporally. The term $\mathrm{t}^{\vartheta-1}$ in the system (9) effectively accounts for non-uniformities in social structures, such as clusters or communities where connections are irregular and not uniformly distributed. As shown in Figure 6, population variations over time are significantly influenced by the fractal dimension. This demonstrates how ϑ adapts the model to reflect real-world complexities, capturing the dynamics of fragmented and heterogeneous environments.

7 Fuzzy Fractal-Fractional Listeriosis Disease Model

In real-world scenarios, uncertainty is inherent and often unavoidable. Mathematical models frequently encounter situations where initial parameters and variables embody such uncertainty. To address this, the application of fuzzy differential modelling becomes essential, as it allows for the incorporation of imprecision and variability into the analytical framework.

Presented below is the fuzzy fractal-fractional differential model of Listeriosis disease, which integrates fuzzy initial conditions $[\tilde{\mathfrak{s}}_0]_\alpha = [\mathrm{s}_0^-(\alpha), \mathrm{s}_0^+(\alpha)]$, $[\tilde{\mathfrak{i}}_0]_\alpha = [\mathrm{i}_0^-(\alpha), \mathrm{i}_0^+(\alpha)]$, $[\tilde{\mathfrak{l}}_0]_\alpha = [\mathfrak{l}_0^-(\alpha), \mathfrak{l}_0^+(\alpha)]$, $[\tilde{\mathfrak{u}}_0]_\alpha = [\mathrm{u}_0^-(\alpha), \mathrm{u}_0^+(\alpha)]$ and $[\tilde{\mathfrak{c}}_0]_\alpha = [\mathrm{c}_0^-(\alpha), \mathrm{c}_0^+(\alpha)]$ to better simulate real-world complexities.

$$
\begin{aligned}
{}^{\varsigma,\vartheta}\mathfrak{D}(\tilde{\mathfrak{s}}) &= \tau^\epsilon \oplus \delta_1^\epsilon(1 \ominus \tilde{\mathfrak{s}} \ominus \tilde{\mathfrak{i}}) \ominus ({}^*\lambda^\epsilon \oplus \tau^\epsilon)\tilde{\mathfrak{s}} \\
{}^{\varsigma,\vartheta}\mathfrak{D}(\tilde{\mathfrak{i}}) &= ({}^*\lambda)^\epsilon\tilde{\mathfrak{s}} \ominus (\delta_2^\epsilon \oplus \tau^\epsilon)\tilde{\mathfrak{i}} \\
{}^{\varsigma,\vartheta}\mathfrak{D}(\tilde{\mathfrak{l}}) &= \sigma^\epsilon\tilde{\mathfrak{l}}(1 \ominus \tilde{\mathfrak{l}}) \\
{}^{\varsigma,\vartheta}\mathfrak{D}(\tilde{\mathfrak{u}}) &= \mu^\epsilon \ominus ({}^*\eta^\epsilon \oplus \mu^\epsilon)\tilde{\mathfrak{u}} \\
{}^{\varsigma,\vartheta}\mathfrak{D}(\tilde{\mathfrak{c}}) &= ({}^*\eta)^\epsilon\tilde{\mathfrak{u}} \ominus \mu^\epsilon\tilde{\mathfrak{c}}
\end{aligned} \tag{17}
$$

Taking α-cut on both sides of the model (17) and applying Definitions 2.4 & 2.5, it is evident that the lower and upper functions of each variable of model (17) can be solved by proceeding in a similar way (6), the required solutions can be represented as:

$$
\begin{aligned}
\tilde{\mathfrak{s}}^-(\mathrm{t}_{\mathrm{j}+1}) = \tilde{\mathfrak{s}}_0^- &+ \frac{(1-\varsigma)\vartheta \mathrm{t}_{\mathrm{j}}^{\vartheta-1}}{\Delta(\varsigma)}\tilde{\psi_1}^-(\mathrm{t}_{\mathrm{j}}, \mathfrak{s}^-, \mathfrak{i}^-, \mathfrak{l}^-, \mathfrak{u}^-, \mathfrak{c}^-) + \frac{\vartheta b^\varsigma}{\Delta(\varsigma)\Gamma(\varsigma+2)} \\
&\times \sum_{n=0}^{\mathrm{j}} \Bigg[\mathrm{t}_n^{\vartheta-1}\tilde{\psi_1}^-(\mathrm{t}_n, \mathfrak{s}^-, \mathfrak{i}^-, \mathfrak{l}^-, \mathfrak{u}^-, \mathfrak{c}^-)\Big((\mathrm{j}+1-n)^\varsigma(\mathrm{j}-n+2+\varsigma) - (\mathrm{j}-n)^\varsigma(\mathrm{j}-n+2+2\varsigma)\Big) \\
&- \mathrm{t}_{n-1}^{\vartheta-1}\tilde{\psi_1}^-(\mathrm{t}_{n-1}, \mathfrak{s}^-, \mathfrak{i}^-, \mathfrak{l}^-, \mathfrak{u}^-, \mathfrak{c}^-)\Big((\mathrm{j}-n+1)^{\varsigma+1} - (\mathrm{j}-n)^\varsigma(\mathrm{j}-n+1+\varsigma)\Big) \Bigg]
\end{aligned}
$$

$$\tilde{\mathfrak{i}}^{-}(\mathrm{t}_{j+1}) = \tilde{\mathfrak{i}}_0^{-} + \frac{(1-\varsigma)\vartheta \mathrm{t}_{\mathrm{j}}^{\vartheta-1}}{\Delta(\varsigma)} \tilde{\psi_2}^{-}(\mathrm{t}_j, \mathfrak{s}^{-}, \mathfrak{i}^{-}, \mathfrak{l}^{-}, \mathfrak{u}^{-}, \mathfrak{c}^{-}) + \frac{\vartheta b^{\varsigma}}{\Delta(\varsigma)\Gamma(\varsigma+2)}$$
$$\times \sum_{n=0}^{\mathrm{j}} \Bigg[\mathrm{t}_n^{\vartheta-1} \tilde{\psi_2}^{-}(\mathrm{t}_n, \mathfrak{s}^{-}, \mathfrak{i}^{-}, \mathfrak{l}^{-}, \mathfrak{u}^{-}, \mathfrak{c}^{-}) \Big((\mathrm{j}+1-n)^{\varsigma}(\mathrm{j}-n+2+\varsigma) - (\mathrm{j}-n)^{\varsigma}(\mathrm{j}-n+2+2\varsigma) \Big)$$
$$- \mathrm{t}_{n-1}^{\vartheta-1} \tilde{\psi_2}^{-}(\mathrm{t}_{n-1}, \mathfrak{s}^{-}, \mathfrak{i}^{-}, \mathfrak{l}^{-}, \mathfrak{u}^{-}, \mathfrak{c}^{-}) \Big((\mathrm{j}-n+1)^{\varsigma+1} - (\mathrm{j}-n)^{\varsigma}(\mathrm{j}-n+1+\varsigma) \Big) \Bigg]$$

$$\tilde{\mathfrak{l}}^{-}(\mathrm{t}_{\mathrm{j}+1}) = \tilde{\mathfrak{l}}_0^{-} + \frac{(1-\varsigma)\vartheta \mathrm{t}_{\mathrm{j}}^{\vartheta-1}}{\Delta(\varsigma)} \tilde{\psi_3}^{-}(\mathrm{t}_{\mathrm{j}}, \mathfrak{s}^{-}, \mathfrak{i}^{-}, \mathfrak{l}^{-}, \mathfrak{u}^{-}, \mathfrak{c}^{-}) + \frac{\vartheta b^{\varsigma}}{\Delta(\varsigma)\Gamma(\varsigma+2)}$$
$$\times \sum_{n=0}^{\mathrm{j}} \Bigg[\mathrm{t}_n^{\vartheta-1} \tilde{\psi_3}^{-}(\mathrm{t}_n, \mathfrak{s}^{-}, \mathfrak{i}^{-}, \mathfrak{l}^{-}, \mathfrak{u}^{-}, \mathfrak{c}^{-}) \Big((\mathrm{j}+1-n)^{\varsigma}(\mathrm{j}-n+2+\varsigma) - (\mathrm{j}-n)^{\varsigma}(\mathrm{j}-n+2+2\varsigma) \Big)$$
$$- \mathrm{t}_{n-1}^{\vartheta-1} \tilde{\psi_3}^{-}(\mathrm{t}_{n-1}, \mathfrak{s}^{-}, \mathfrak{i}^{-}, \mathfrak{l}^{-}, \mathfrak{u}^{-}, \mathfrak{c}^{-}) \Big((\mathrm{j}-n+1)^{\varsigma+1} - (\mathrm{j}-n)^{\varsigma}(\mathrm{j}-n+1+\varsigma) \Big) \Bigg]$$

$$\tilde{\mathfrak{u}}^{-}(\mathrm{t}_{\mathrm{j}+1}) = \tilde{\mathfrak{u}}_0^{-} + \frac{(1-\varsigma)\vartheta \mathrm{t}_{\mathrm{j}}^{\vartheta-1}}{\Delta(\varsigma)} \tilde{\psi_4}^{-}(\mathrm{t}_{\mathrm{j}}, \mathfrak{s}^{-}, \mathfrak{i}^{-}, \mathfrak{l}^{-}, \mathfrak{u}^{-}, \mathfrak{c}^{-}) + \frac{\vartheta b^{\varsigma}}{\Delta(\varsigma)\Gamma(\varsigma+2)}$$
$$\times \sum_{n=0}^{\mathrm{j}} \Bigg[\mathrm{t}_n^{\vartheta-1} \tilde{\psi_4}^{-}(\mathrm{t}_{\mathrm{j}}, \mathfrak{s}^{-}, \mathfrak{i}^{-}, \mathfrak{l}^{-}, \mathfrak{u}^{-}, \mathfrak{c}^{-}) \Big((\mathrm{j}+1-n)^{\varsigma}(\mathrm{j}-n+2+\varsigma) - (\mathrm{j}-n)^{\varsigma}(\mathrm{j}-n+2+2\varsigma) \Big)$$
$$- \mathrm{t}_{n-1}^{\vartheta-1} \tilde{\psi_4}^{-}(\mathrm{t}_{n-1}, \mathfrak{s}^{-}, \mathfrak{i}^{-}, \mathfrak{l}^{-}, \mathfrak{u}^{-}, \mathfrak{c}^{-}) \Big((\mathrm{j}-n+1)^{\varsigma+1} - (\mathrm{j}-n)^{\varsigma}(\mathrm{j}-n+1+\varsigma) \Big) \Bigg]$$

$$\tilde{\mathfrak{c}}^{-}(\mathrm{t}_{\mathrm{j}+1}) = \tilde{\mathfrak{c}}_0^{-} + \frac{(1-\varsigma)\vartheta \mathrm{t}_{\mathrm{j}}^{\vartheta-1}}{\Delta(\varsigma)} \tilde{\psi_5}^{-}(\mathrm{t}_{\mathrm{j}}, \mathfrak{s}^{-}, \mathfrak{i}^{-}, \mathfrak{l}^{-}, \mathfrak{u}^{-}, \mathfrak{c}^{-}) + \frac{\vartheta b^{\varsigma}}{\Delta(\varsigma)\Gamma(\varsigma+2)}$$
$$\times \sum_{n=0}^{\mathrm{j}} \Bigg[\mathrm{t}_n^{\vartheta-1} \tilde{\psi_5}^{-}(\mathrm{t}_n, \mathfrak{s}^{-}, \mathfrak{i}^{-}, \mathfrak{l}^{-}, \mathfrak{u}^{-}, \mathfrak{c}^{-}) \Big((\mathrm{j}+1-n)^{\varsigma}(\mathrm{j}-n+2+\varsigma) - (\mathrm{j}-n)^{\varsigma}(\mathrm{j}-n+2+2\varsigma) \Big)$$
$$- \mathrm{t}_{n-1}^{\vartheta-1} \tilde{\psi_5}^{-}(\mathrm{t}_{n-1}, \mathfrak{s}^{-}, \mathfrak{i}^{-}, \mathfrak{l}^{-}, \mathfrak{u}^{-}, \mathfrak{c}^{-}) \Big((\mathrm{j}-n+1)^{\varsigma+1} - (\mathrm{j}-n)^{\varsigma}(\mathrm{j}-n+1+\varsigma) \Big) \Bigg]$$

$$\tilde{\mathfrak{s}}^{+}(\mathrm{t}_{\mathrm{j}+1}) = \tilde{\mathfrak{s}}_0^{+} + \frac{(1-\varsigma)\vartheta \mathrm{t}_{\mathrm{j}}^{\vartheta-1}}{\Delta(\varsigma)} \tilde{\psi_1}^{+}(\mathrm{t}_{\mathrm{j}}, \mathfrak{s}^{+}, \mathfrak{i}^{+}, \mathfrak{l}^{+}, \mathfrak{u}^{+}, \mathfrak{c}^{+}) + \frac{\vartheta b^{\varsigma}}{\Delta(\varsigma)\Gamma(\varsigma+2)}$$
$$\times \sum_{n=0}^{\mathrm{j}} \Bigg[\mathrm{t}_n^{\vartheta-1} \tilde{\psi_1}^{+}(\mathrm{t}_n, \mathfrak{s}^{+}, \mathfrak{i}^{+}, \mathfrak{l}^{+}, \mathfrak{u}^{+}, \mathfrak{c}^{+}) \Big((\mathrm{j}+1-n)^{\varsigma}(\mathrm{j}-n+2+\varsigma) - (\mathrm{j}-n)^{\varsigma}(\mathrm{j}-n+2+2\varsigma) \Big)$$
$$- \mathrm{t}_{n-1}^{\vartheta-1} \tilde{\psi_1}^{+}(\mathrm{t}_{n-1}, \mathfrak{s}^{+}, \mathfrak{i}^{+}, \mathfrak{l}^{+}, \mathfrak{u}^{+}, \mathfrak{c}^{+}) \Big((\mathrm{j}-n+1)^{\varsigma+1} - (\mathrm{j}-n)^{\varsigma}(\mathrm{j}-n+1+\varsigma) \Big) \Bigg]$$

$$\tilde{\mathfrak{i}}^{+}(\mathrm{t}_{j+1}) = \tilde{\mathfrak{i}}_0^{+} + \frac{(1-\varsigma)\vartheta \mathrm{t}_{\mathrm{j}}^{\vartheta-1}}{\Delta(\varsigma)} \tilde{\psi_2}^{+}(\mathrm{t}_j, \mathfrak{s}^{+}, \mathfrak{i}^{+}, \mathfrak{l}^{+}, \mathfrak{u}^{+}, \mathfrak{c}^{+}) + \frac{\vartheta b^{\varsigma}}{\Delta(\varsigma)\Gamma(\varsigma+2)}$$
$$\times \sum_{n=0}^{\mathrm{j}} \Bigg[\mathrm{t}_n^{\vartheta-1} \tilde{\psi_2}^{+}(\mathrm{t}_n, \mathfrak{s}^{+}, \mathfrak{i}^{+}, \mathfrak{l}^{+}, \mathfrak{u}^{+}, \mathfrak{c}^{+}) \Big((\mathrm{j}+1-n)^{\varsigma}(\mathrm{j}-n+2+\varsigma) - (\mathrm{j}-n)^{\varsigma}(\mathrm{j}-n+2+2\varsigma) \Big)$$
$$- \mathrm{t}_{n-1}^{\vartheta-1} \tilde{\psi_2}^{+}(\mathrm{t}_{n-1}, \mathfrak{s}^{+}, \mathfrak{i}^{+}, \mathfrak{l}^{+}, \mathfrak{u}^{+}, \mathfrak{c}^{+}) \Big((\mathrm{j}-n+1)^{\varsigma+1} - (\mathrm{j}-n)^{\varsigma}(\mathrm{j}-n+1+\varsigma) \Big) \Bigg]$$

$$
\begin{aligned}
\tilde{\mathfrak{l}}^{+}(\mathrm{t}_{\mathrm{j}+1}) &= \tilde{\mathfrak{l}}_0^{+} + \frac{(1-\varsigma)\vartheta \mathrm{t}_{\mathrm{j}}^{\vartheta-1}}{\Delta(\varsigma)} \tilde{\psi_3}^{+}(\mathrm{t}_{\mathrm{j}}, \mathfrak{s}^{+}, \mathfrak{i}^{+}, \mathfrak{l}^{+}, \mathfrak{u}^{+}, \mathfrak{c}^{+}) + \frac{\vartheta b^{\varsigma}}{\Delta(\varsigma)\Gamma(\varsigma+2)} \\
&\quad \times \sum_{n=0}^{\mathrm{j}} \Bigg[\mathrm{t}_n^{\vartheta-1} \tilde{\psi_3}^{+}(\mathrm{t}_n, \mathfrak{s}^{+}, \mathfrak{i}^{+}, \mathfrak{l}^{+}, \mathfrak{u}^{+}, \mathfrak{c}^{+}) \Big((\mathrm{j}+1-n)^{\varsigma}(\mathrm{j}-n+2+\varsigma) - (\mathrm{j}-n)^{\varsigma}(\mathrm{j}-n+2+2\varsigma) \Big) \\
&\quad - \mathrm{t}_{n-1}^{\vartheta-1} \tilde{\psi_3}^{+}(\mathrm{t}_{n-1}, \mathfrak{s}^{+}, \mathfrak{i}^{+}, \mathfrak{l}^{+}, \mathfrak{u}^{+}, \mathfrak{c}^{+}) \Big((\mathrm{j}-n+1)^{\varsigma+1} - (\mathrm{j}-n)^{\varsigma}(\mathrm{j}-n+1+\varsigma) \Big) \Bigg] \\
\tilde{\mathfrak{u}}^{+}(\mathrm{t}_{\mathrm{j}+1}) &= \tilde{\mathfrak{u}}_0^{+} + \frac{(1-\varsigma)\vartheta \mathrm{t}_{\mathrm{j}}^{\vartheta-1}}{\Delta(\varsigma)} \tilde{\psi_4}^{+}(\mathrm{t}_{\mathrm{j}}, \mathfrak{s}^{+}, \mathfrak{i}^{+}, \mathfrak{l}^{+}, \mathfrak{u}^{+}, \mathfrak{c}^{+}) + \frac{\vartheta b^{\varsigma}}{\Delta(\varsigma)\Gamma(\varsigma+2)} \\
&\quad \times \sum_{n=0}^{\mathrm{j}} \Bigg[\mathrm{t}_n^{\vartheta-1} \tilde{\psi_4}^{+}(\mathrm{t}_n, \mathfrak{s}^{+}, \mathfrak{i}^{+}, \mathfrak{l}^{+}, \mathfrak{u}^{+}, \mathfrak{c}^{+}) \Big((\mathrm{j}+1-n)^{\varsigma}(\mathrm{j}-n+2+\varsigma) - (\mathrm{j}-n)^{\varsigma}(\mathrm{j}-n+2+2\varsigma) \Big) \\
&\quad - \mathrm{t}_{n-1}^{\vartheta-1} \tilde{\psi_4}^{+}(\mathrm{t}_{n-1}, \mathfrak{s}^{+}, \mathfrak{i}^{+}, \mathfrak{l}^{+}, \mathfrak{u}^{+}, \mathfrak{c}^{+}) \Big((\mathrm{j}-n+1)^{\varsigma+1} - (\mathrm{j}-n)^{\varsigma}(\mathrm{j}-n+1+\varsigma) \Big) \Bigg] \\
\tilde{\mathfrak{c}}^{+}(\mathrm{t}_{\mathrm{j}+1}) &= \tilde{\mathfrak{c}}_0^{+} + \frac{(1-\varsigma)\vartheta \mathrm{t}_{\mathrm{j}}^{\vartheta-1}}{\Delta(\varsigma)} \tilde{\psi_5}^{+}(\mathrm{t}_{\mathrm{j}}, \mathfrak{s}^{+}, \mathfrak{i}^{+}, \mathfrak{l}^{+}, \mathfrak{u}^{+}, \mathfrak{c}^{+}) + \frac{\vartheta b^{\varsigma}}{\Delta(\varsigma)\Gamma(\varsigma+2)} \\
&\quad \times \sum_{n=0}^{\mathrm{j}} \Bigg[\mathrm{t}_n^{\vartheta-1} \tilde{\psi_5}^{+}(\mathrm{t}_n, \mathfrak{s}^{+}, \mathfrak{i}^{+}, \mathfrak{l}^{+}, \mathfrak{u}^{+}, \mathfrak{c}^{+}) \Big((\mathrm{j}+1-n)^{\varsigma}(\mathrm{j}-n+2+\varsigma) - (\mathrm{j}-n)^{\varsigma}(\mathrm{j}-n+2+2\varsigma) \Big) \\
&\quad - \mathrm{t}_{n-1}^{\vartheta-1} \tilde{\psi_5}^{+}(\mathrm{t}_{n-1}, \mathfrak{s}^{+}, \mathfrak{i}^{+}, \mathfrak{l}^{+}, \mathfrak{u}^{+}, \mathfrak{c}^{+}) \Big((\mathrm{j}-n+1)^{\varsigma+1} - (\mathrm{j}-n)^{\varsigma}(\mathrm{j}-n+1+\varsigma) \Big) \Bigg]
\end{aligned}
\tag{18}
$$

7.1 Fuzzy Fractal-Fractional Model Results

The solutions (18) have been evaluated through MATLAB for several values of ς & ϑ with initial conditions $[\tilde{\mathfrak{s}}_0]_\alpha = [0.57 + 0.03\alpha, 0.63 - 0.03\alpha]$, $[\tilde{\mathfrak{i}}_0]_\alpha = [0.27 + 0.03\alpha, 0.33 - 0.03\alpha]$, $[\tilde{\mathfrak{l}}_0]_\alpha = [0.4 + 0.05\alpha, 0.5 - 0.05\alpha]$, $[\tilde{\mathfrak{u}}_0]_\alpha = [0.65 + 0.05\alpha, 0.75 - 0.05\alpha]$ and $[\tilde{\mathfrak{c}}_0]_\alpha = 1 \ominus [\tilde{\mathfrak{u}}_0]_\alpha$ and the results obtained for $\alpha = 0$ are discussed. Figure 8 illustrates the fuzzy initial conditions. By applying the α-cut method to the fuzzy system, the model is systematically decomposed into a family of interval-valued differential equations, each corresponding to a fixed α-level. This transformation yields deterministic lower and upper bound systems, which are then solved numerically using the same fractal-fractional operator. The interval-valued solutions obtained accurately reflect the uncertainty associated with the fuzzy formulation at each α-cut. The fuzzy trajectories for each population compartment exhibit consistent variation between their lower and upper bounds, revealing the effect of uncertainty on the system dynamics. Hence, the embedding strategy not only simplifies the computational treatment of the fuzzy system but also ensures theoretical consistency through the α-cut representation, thereby validating the modelling approach adopted in this work. Figure 7 reveals that,

- The susceptible population $\mathcal{H}_s(\mathrm{t})$ decreases over time, with lower and upper bounds highlighting the range of expected reductions.

- The infected population $\mathcal{H}_i(\mathrm{t})$ initially increases, peaks, and then declines, with lower and upper bounds reflecting variability in infection dynamics.

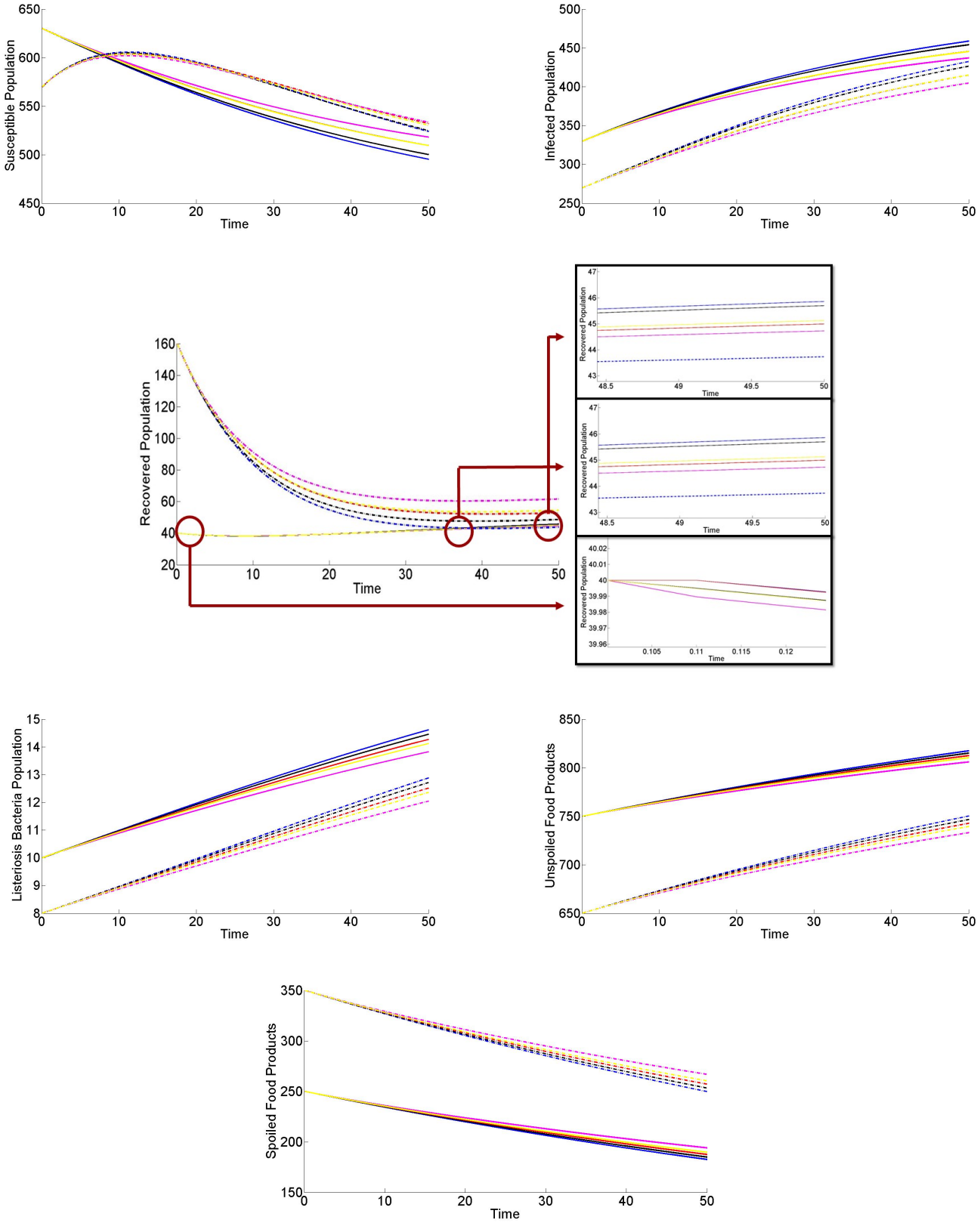

Figure 7: Fuzzy Population Dynamics for varying ς and ϑ; Solid lines represent the upper bound and dotted lines represent the lower bound of the solutions.

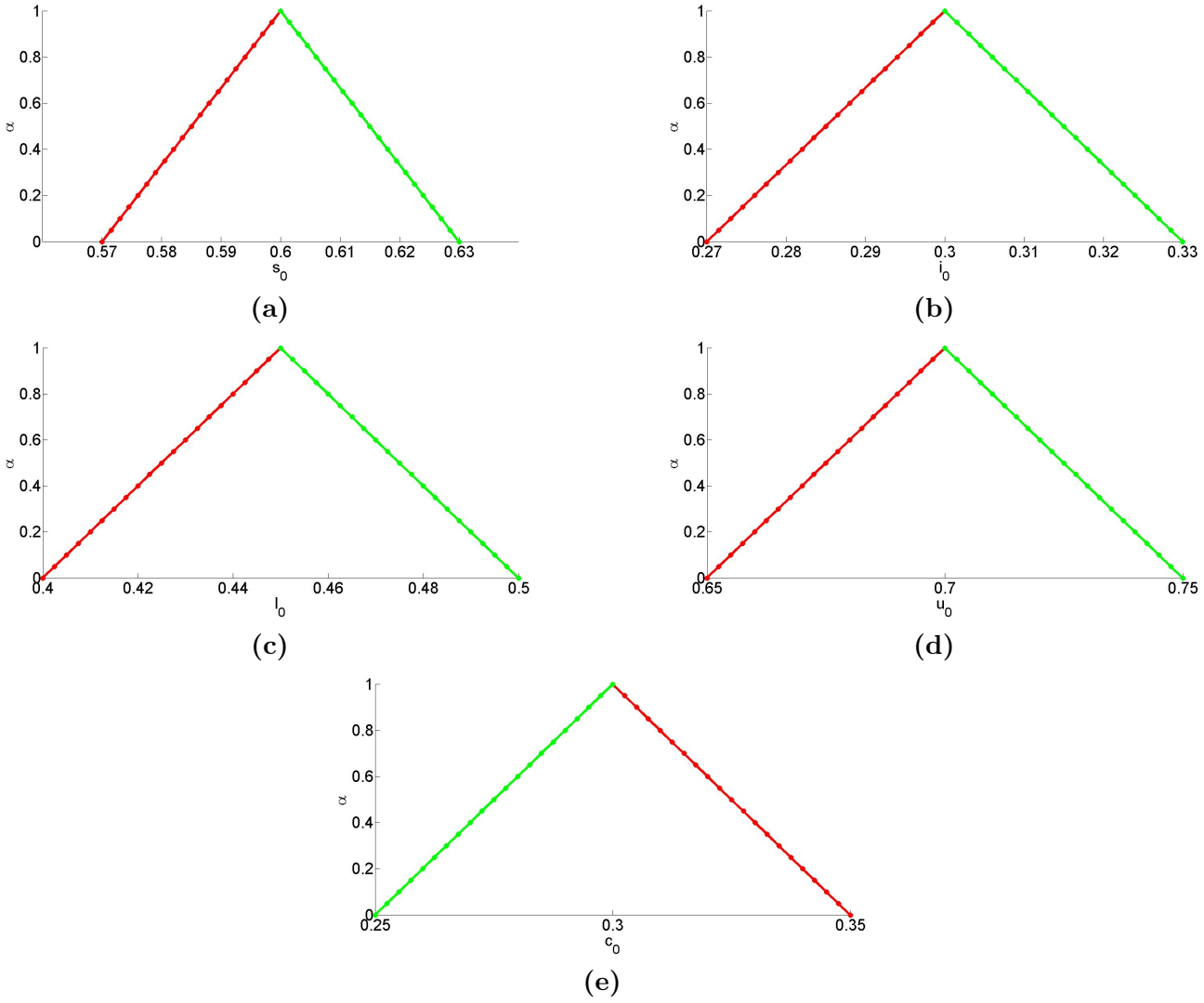

Figure 8: Fuzzy Initial conditions for $\alpha \in [0,1]$

- The recovered population $\mathcal{H}_r(\mathrm{t})$ shows an upward trend, with lower and upper bounds indicating the range of expected recoveries.
- The Listeriosis bacteria population $\mathcal{L}(\mathrm{t})$ decreases significantly, with lower and upper bounds capturing the variability in bacterial dynamics.
- The unspoiled food $\mathcal{U}(\mathrm{t})$ decreases, while the spoiled food $\mathcal{C}(\mathrm{t})$ increases over time, with respective lower and upper bounds highlighting the uncertainty in food contamination and spoilage dynamics.

This comprehensive analysis underscores the importance of considering both lower and upper solutions to account for uncertainties in the model parameters, offering a more accurate representation of the disease's behaviour. In this work, fuzzy numbers are represented using their parametric form, where each fuzzy quantity is described at every $\alpha \in [0, 1]$ by a closed interval. All fuzzy computations, including differential operations, are performed through their α-cut representations, ensuring consistency and interpretability across the entire fuzzy domain. To compute differences between two fuzzy numbers, the generalized difference formulation

in Definition 2.5 guarantees that the resulting set remains a valid interval at each α-level and utilizes a computationally efficient method consistent with parametric fuzzy arithmetic. This method has also been validated through the results in Figure 7, where the evolution of each compartment under uncertainty is clearly bounded by lower and upper solutions derived from the parametric structure.

8 Conclusion

The study demonstrates the utility of combining fractal-fractional differential equations and fuzzy logic to model and analyse the complex dynamics of listeriosis. By incorporating fractal calculus, the model captures intricate, multi-scale behaviours that reflect real-world disease transmission more accurately than traditional models. The inclusion of fuzzy initial conditions addresses the inherent uncertainties in initial parameters, enhancing the robustness and predictive power of the analysis.

Key properties, such as existence, uniqueness, and Ulam-Hyers stability, affirm the mathematical soundness of the model, ensuring reliable outcomes. Computational simulations show that variations in fractional orders and fractal dimensions significantly influence the spread of infection and the overall behaviour of the population dynamics. This provides valuable insights for designing targeted intervention strategies.

The fuzzy fractal-fractional approach adds depth by simulating a realistic range of scenarios, capturing potential fluctuations, and supporting more informed decision-making under uncertain conditions. This methodological advancement illustrates the potential for broader application in epidemic modelling and public health policy.

In conclusion, the integration of fractal-fractional calculus and fuzzy systems in disease modelling marks a significant step forward in understanding and controlling complex public health issues like listeriosis. The approach presented not only reinforces the need for advanced mathematical tools in epidemiology, but also paves the way for future studies that can further refine these models to address other infectious diseases and uncertainties in real-world data.

Acknowledgements: "The article has been written with the financial support of Alagappa University Research Fund sanctioned vide Letter No. Ph.D./R20163154/AURF Fellowship/2024."

Conflict of Interest: "The authors declare no conflict of interest."

References

[1] Koopmans MM, Brouwer MC, Vázquez-Boland JA, van de Beek D. Human listeriosis. *Clinical Microbiology Reviews*. 2023; 36(1): e00060-19. https://doi.org/10.1128/cmr.00060-19

[2] World Health Organization. *International travel and health*. https://www.who.int/ith/diseases/Listeriosis [Accessed 26th July 2020]

[3] Riaz R, Shaheen R. Listeriosis in pregnancy: an important cause of febrile illness Listeriosis in pregnancy: an important cause of febrile illness. *Journal of University Medical & Dental College*. 2022; 13(1): 351-353. https://doi.org/10.37723/jumdc.v13i1.709

[4] Ivanek R, Gröhn YT, Wiedmann M. Listeria monocytogenes in multiple habitats and host populations: review of available data for mathematical modeling. *Foodbourne Pathogens & Disease*. 2006; 3(4): 319-336. https://doi.org/10.1089/fpd.2006.3.319

[5] Swaminathan B, Gerner-Smidt P. The epidemiology of human listeriosis. *Microbes and Infection*. 2007; 9(10): 1236-1243. https://doi.org/10.1016/j.micinf.2007.05.011

[6] Hernandez-Milian A, Payeras-Cifre A. What is new in listeriosis?. *BioMed Research International*. 2014; 2014(1): 358051. https://doi.org/10.1155/2014/358051

[7] Bennion JR, Sorvillo F, Wise ME, Krishna S, Mascola L. Decreasing listeriosis mortality in the United States, 1990-2005. *Clinical Infectious Diseases*. 2008; 47(7): 867-874. https://doi.org/10.1086/591131

[8] Bongiovanni M, Cavallo C, Barda B, Strulak L, Bernasconi E, Cardia A. Clinical findings of listeria monocytogenes infections with a sSpecial focus on bone localizations. *Microorganisms*. 2024; 12(1): 178. https://doi.org/10.3390/microorganisms12010178

[9] Duarte F, Pinto SM, et al. A rare presentation of Listeria monocytogenes infection: perianal abscess associated with lumbar spine osteitis. *IDCases*. 2019; 15: e00488. https://doi.org/10.1016/j.idcr.2019.e00488

[10] Centers for disease Control and Prevention. [Accessed 26 May 2020] https://www.cdc.gov/Listeria/prevention.html

[11] Roh SH, Oh YJ, Lee SY, Kang JH, Min SC. Inactivation of Escherichia coli O157: H7, Salmonella, Listeria monocytogenes, and Tulane virus in processed chicken breast via atmospheric in-package cold plasma treatment. *LWT* 2020; 127: 109429. http://doi.org/10.1016/j.lwt.2020.109429

[12] Ryser ET, Marth EH. *Listeria, listeriosis, and food safety*. 3rd ed. Boca Raton: CRC Press; 2007. https://doi.org/10.1201/9781420015188

[13] Shi C, Lv D, Zhou K, Jin T, Wang G, Wang B, Li Y, Xu Y. Clinical and laboratory characteristics of patients infected by Listeria monocytogenes at a Tertiary hospital in Hefei City, China. *Infection and Drug Resistance*. 2021; 2021: 4409-4419. https://doi.org/10.2147/IDR.S334929

[14] Kaptchouang Tchatchouang CD, Fri J, De Santi M, Brandi G, Schiavano GF, Amagliani G, Ateba CN. Listeriosis outbreak in South Africa: a comparative analysis with previously reported cases worldwide. *Microorganisms*. 2020; 8(1): 135. https://doi.org/10.3390/microorganisms8010135

[15] Sulieman AME, Abu Zeid IM, Abdalla EM, Ed-Dra A. New discoveries in toxins from Gram-Positive Bacteria, Listeria monocytogenes. In: Moneim Elhadi Sulieman, A., Alshammari, N.I. (eds.) *Microbial toxins in food systems: causes, mechanisms, complications, and metabolism*. Cham: Springer; 2024. p. 303-318. https://doi.org/10.1007/978-3-031-62839-9_23

[16] Chukwu CW, Nyabadza F, Asamoah JKK. A mathematical model and optimal control for Listeriosis disease from ready-to-eat food products. *International Journal of Computing Science and Mathematics*. 2023; 17(1): 39-49. https://doi.org/10.1504/IJCSM.2023.130421

[17] Lanzas C, Lu Z, Gröhn YT. Mathematical modeling of the transmission and control of foodborne pathogens and antimicrobial resistance at preharvest. *Foodborne Pathogens and Disease*. 2011; 8(1): 1-0. https://doi.org/10.1089/fpd.2010.0643

[18] Osman S, Makinde OD. A mathematical model for coinfection of listeriosis and anthrax diseases. *International Journal of Mathematics and Mathematical Sciences*. 2018; 2018(1): 1725671. https://doi.org/10.1155/2018/1725671

[19] Osman S, Otoo D, Sebil C. Analysis of listeriosis transmission dynamics with optimal control. *Applied Mathematics*. 2020; 11(7): 712-737. https://doi.org/10.4236/am.2020.117048

[20] Osman S, Makinde OD, Theuri DM. Stability analysis and modelling of listeriosis dynamics in human and animal populations. *Global Journal of Pure and Applied Mathematics*. 2018; 14(1): 115-137.

[21] Bonyah E, Yavuz M, Baleanu D, Kumar S. A robust study on the listeriosis disease by adopting fractal-fractional operators. *Alexandria Engineering Journal*. 2022; 61(3): 2016-2028. https://doi.org/10.1016/j.aej.2021.07.010

[22] Chukwu CW, Nyabadza F. A theoretical model of listeriosis driven by cross contamination of ready-to-eat food products. *International Journal of Mathematics and Mathematical Sciences*. 2020; 2020(1): 9207403. https://doi.org/10.1155/2020/9207403

[23] Tchoumi SY, Chukwu CW, Windarto AP. A multi-population approach to epidemiological modeling of listeriosis transmission dynamics incorporating food and environmental contamination. *Healthcare Analytics*. 2024; 5: 100344. https://doi.org/10.1016/j.health.2024.100344

[24] Osman S, Makinde OD, Theuri DM. Mathematical modelling of Listeriosis Epidemics in Animal and Human Population with Optimal Control. *Tamkang Journal of Mathematics*. 2020; 51(4): 261-287. https://doi.org/10.5556/j.tkjm.51.2020.2860

[25] Chauhan JP, Khirsariya SR, Yeolekar BM, Yeolekar MA. Fractional mathematical model of Listeria infection caused by pre-cooked package food. *Results in Control and Optimization*. 2024; 14: 100371. https://doi.org/10.1016/j.rico.2024.100371

[26] Asamoah JKK, Addai E, Arthur YD, Okyere E. A fractional mathematical model for listeriosis infection using two kernels. *Decision Analytics Journal*. 2023; 6:100191. https://doi.org/10.1016/j.dajour.2023.100191

[27] Atangana A. Fractal-fractional differentiation and integration: connecting fractal calculus and fractional calculus to predict complex system. *Chaos, Solitons & Fractals*. 2017; 102: 396-406. https://doi.org/10.1016/j.chaos.2017.04.027

[28] Kubra KT, Gulshan S, Ali R. An Atangana-Baleanu derivative-based fractal-fractional order model for the monkey pox virus: A case study of USA. *Partial Differential Equations in Applied Mathematics*. 2024; 9: 100623. https://doi.org/10.1016/j.padiff.2024.100623

[29] Atangana A, Qureshi S. Modeling attractors of chaotic dynamical systems with fractalfractional operators. *Chaos, Solitons & Factals*. 2019; 123: 320-337. https://doi.org/10.1016/j.chaos.2019.04.020

[30] Qureshi S, Atangana A. Fractal-fractional differentiation for the modeling and mathematical analysis of nonlinear diarrhea transmission dynamics under the use of real data. *Chaos, Solitons & Fractals*. 2020; 136: 109812. https://doi.org/10.1016/j.chaos.2020.109812

[31] Kubra KT, Ali R, Alqahtani RT, Gulshan S, Iqbal Z. Author Correction: analysis and comparative study of a deterministic mathematical model of SARS-COV-2 with fractal-fractional operators: a case study. *Scientific Reports*. 2024; 14(1): 6431. https://doi.org/10.1038/s41598-024-58414-y

[32] Nisar KS, Ahmad S, Ullah A, Shah K, Alrabaiah H, Arfan M. Mathematical analysis of SIRD model of COVID-19 with Caputo fractional derivative based on real data. *Results in Physics*. 2021; 21: 103772. https://doi.org/10.1016/j.rinp.2020.103772

[33] Qureshi S, Yusuf A. Modeling chickenpox disease with fractional derivatives: from Caputo to Atangana-Baleanu. *Chaos, Solitons & Fractals*. 2019; 122: 111-118. https://doi.org/10.1016/j.chaos.2019.03.020

[34] Singh HK, Pandey DN. Analysis of the Chickenpox Disease Evolution in an MSEIR Model Using Fractal-Fractional Differential Operator. *Differential Equations and Dynamical Systems*. 2024; 4: 1-21. https://doi.org/10.1007/s12591-024-00690-1

[35] Allahviranloo, T. *Fuzzy fractional differential operators and equations*. Cham: Springer; 2021. https://doi.org/10.1007/978-3-030-51272-9

[36] Babakordi F, Allahviranloo T. Application of fuzzy ABC fractional differential equations in infectious diseases. *Computational Methods for Differential Equations*. 2024; 12(1): 1-15. https://doi.org/10.22034/cmde.2023.47768.2000

[37] Subramanian S, Kumaran A, Ravichandran S, Venugopal P, Dhahri S, Ramasamy K. Fuzzy fractional Caputo derivative of susceptible-infectious-removed epidemic model for childhood diseases. *Mathematics*. 2024; 12(3): 466. https://doi.org/10.3390/math12030466

[38] Babakordi F. An efficient method for solving the fuzzy AH1N1/09 influenza model using the fuzzy Atangana-Baleanu-Caputo fractional derivative. *Fuzzy Optimization and Modeling Journal*. 2023; 4(2): 27-38. https://doi.org/10.30495/fomj.2023.1988760.1096

[39] Khaliq R, Iqbal P, Bhat SA, Sheergojri AR. A fuzzy mathematical model for tumor growth pattern using generalized Hukuhara derivative and its numerical analysis. *Applied Soft Computing*. 2022; 118: 108467. https://doi.org/10.1016/j.asoc.2022.108467

[40] Granas A, Dugundji J. *Fixed point theory*. New York: Springer Monographs in Mathematics/Springer-Verlag; 2003. https://doi.org/10.1007/978-0-387-21593-8

Tamil Vizhi Mariappan
Department of Mathematics
Alagappa University
Karaikudi, India.
E-mail: tamilvizhi2502@gmail.com

Vimala Jayakumar
Department of Mathematics
Alagappa University
Karaikudi, India.
E-mail: vimaljey@alagappauniversity.ac.in

Jeevitha Kannan
Department of Mathematics
Alagappa University
Karaikudi, India.
E-mail: kjeevitha991@gmail.com

© By the Authors. Published by Islamic Azad University, Bandar Abbas Branch. This article is an open-access article distributed under the terms and conditions of the Creative Commons Attribution 4.0 International (CC BY 4.0) http://creativecommons.org/licenses/by/4.0/.